INFORMATION TO USERS

This manuscript has been reproduced from the microfilm master. UMI films the text directly from the original or copy submitted. Thus, some thesis and dissertation copies are in typewriter face, while others may be from any type of computer printer.

The quality of this reproduction is dependent upon the quality of the copy submitted. Broken or indistinct print, colored or poor quality illustrations and photographs, print bleedthrough, substandard margins, and improper alignment can adversely affect reproduction.

In the unlikely event that the author did not send UMI a complete manuscript and there are missing pages, these will be noted. Also, if unauthorized copyright material had to be removed, a note will indicate the deletion.

Oversize materials (e.g., maps, drawings, charts) are reproduced by sectioning the original, beginning at the upper left-hand corner and continuing from left to right in equal sections with small overlaps.

Photographs included in the original manuscript have been reproduced xerographically in this copy. Higher quality 6" x 9" black and white photographic prints are available for any photographs or illustrations appearing in this copy for an additional charge. Contact UMI directly to order.

ProQuest Information and Learning
300 North Zeeb Road, Ann Arbor, MI 48106-1346 USA
800-521-0600

Interconnection of a 2D vertical-cavity surface-emitting laser array to a receiver array via a fiber image guide

Tomasz Maj

McGill
Faculty of Engineering

Department of Electrical and Computer Engineering
McGill University
Montréal, Québec, Canada
November, 1999

A thesis submitted to the Faculty of Graduate Studies and Research in partial fulfillment of the requirements of the degree of Master of Engineering

Abstract

Parallel Optical Data Links (PODLs) have the potential to solve interconnection bottlenecks which are currently being experienced in high-speed communication and information processing systems. Such links often require a large number of channels and two-dimensional arrays of active optoelectronic devices are being developed. In order to interconnect these devices, fiber image guide technology consisting of a bundle of several thousand equally spaced optical fibers is being proposed to alleviate the need for dedicated fibers.

This thesis examines the implementation of a two-dimensional parallel optical interconnect consisting of an array of Vertical-Cavity Surface-Emitting Lasers (VCSELs), a 1.35m Fiber Image Guide (FIG) and a Metal-Semiconductor-Metal (MSM) receiver array. Coupling issues associated with image guides are analysed and discussed as well as general image guide properties and transmission characteristics. The design, construction and integration aspects of the data link, including optics, electronics and optomechanics are summarised. Characterization results are presented and a transmission rate of 250 Mbit/s per channel is demonstrated with an optical crosstalk of less than –27 dB and a total optical loss of -3dB.

Sommaire

Les liens parallèles optiques de communication ont le potentiel de résoudre plusieurs limitations d'interconnection qui existe actuellement dans les systèmes à haute vitesse de communication et de traitement de données. Ces liens nécessitent souvent un grand nombre de canaux parallèles et des matrices opto-électroniques bi–dimentionnelles sont en dévelopement. Pour faire un lien entre les puces opto-électroniques, la technologie de guide d'image, basée sur un groupement de quelques milliers de fibres optiques équidistantes, est proposée comme alternative à des fibres individuelles.

Cette thèse examine la réalisation d'un lien parallèle optique bi-dimensionnel basé sur une matrice de lasers à cavité verticale avec émission de surface (VCSEL), un guide d'image de 1.35 m et une matrice de détecteurs Métal-Semiconducteur-Métal (MSM). La qualité du couplage optique dans le guide d'image est analysée et discutée ainsi que les propriétés générales et les charactéristiques de transmission du guide d'image. Les aspects de la conception, de la construction et de l'integration de l'interconnection incluant l'optique, l'électronique et l'optoméchanique sont résumés. Les résultats de la charactérisation sont présentés et une vitesse de transmission de 250 Mbit/s par canal est démontrée avec une interférence optique de moins de –27 dB et une perte totale de -3 dB.

Acknowledgements

My most sincere thanks to Professor Andrew Kirk for his advice, guidance and encouragement over the course of my thesis. Not only was I given an opportunity to be part of a great research group, but also to work on some truly interesting and rewarding projects. I am also grateful to Professor David Plant for his constant support and continuous advice.

Special thanks to Marc Châteauneuf, with whom I shared the office, for his friendship and many helpful discussions we held together. Many thanks to Mike Ayliffe, Eric Bernier, Mike Venditti and David Rolston for their technical assistance and suggestions.

I would also like to extend my thank you to the rest of the graduate students of the photonics systems group, for creating a professional and pleasant working environment: Alan, Daniel, Emmanuelle, Eric, Feras, Fred, Fred, Greg, Julianna, Julien, Keivan, Leo, Madeleine, Mitch, Pritam, and Xin.

Thanks to Joe Ahadian and Professor Clifton Fonstad for providing me with the most needed receiver arrays. Thanks to those at the CITR office and at the mechanical workshop.

Finally, I would like to thank my parents for their constant love and support throughout my life.

The research at McGill was supported by the Canadian Institute for Telecommunications Research under the National Centers of Excellence program of Canada, the National Sciences and Engineering Research Council (NSERC) (OGP0194547) and Fonds pour la Formation de Chercheurs et l'Aide à la Recherche (FCAR) (NC-1778). Funding for the fabrication of the receiver array was provided by the Optoelectronic Industry Development Association (OIDA).

Table of Contents

Chapter 1

Introduction

1.1 Motivation

The tremendous development of information processing systems has created a necessity for higher speed and higher density wiring between these processing units. One visible trend in computer technology is that the Central Processing Unit (CPU) speed continues to push towards the 1 GHz regime. At the same time, CPUs are processing data in larger parallel formats [1] and computer bus widths possessing 128 channels or more may be required in the near future. Optical interconnection technology is now drawing a wide attention as the most promising candidate to overcome those bottlenecks.

Currently, the use of optical networks is widespread only in long-haul telecommunications, such as telephone and data communication national trunk lines, and high throughput analog broadcast systems, such as cable TV. Technological advances in high-bandwidth single mode fiber optics and in wavelength division multiplexing (WDM) technology have justified the cost for the deployment of such systems. These long-haul systems have been demonstrated to provide a total capacity of 2.6 Tbits/s per fiber and over 120 km [2].

With the increase of demand in data by the development of the internet and digital multimedia communications, light wave carriers are beginning to replace standard copper and other metallic interconnects in systems of ever decreasing size. System designers at all levels are beginning to see performance limits of metallic cables and open the possibility to use high bandwidth optical interconnections. These interconnections will improve system performance; initially starting with local-area networks [3], later migrating to computer system backplanes [4], and even onto VLSI chips (chip-to-chip).

Figure 1.1 provides a perspective on the conventional digital interconnection hierarchy and their typical lengths. Current interconnections for shelves, boards and backplanes are still mainly provided electrically using electrical backplanes, flex-PCBs or cabling. The advancements in chip-sets performing beyond 1 Gbit/s and in larger parallel formats will require electrical components to be manufactured with better shielding, more expensive low-loss dielectrics and boards with tighter requirements on quality and flatness. Due to the increased complexity and cost associated with the development electrical solutions, various interconnection alternatives are being researched, including free-space optics, individual fiber based arrays, polymer waveguides, and fiber image guides.

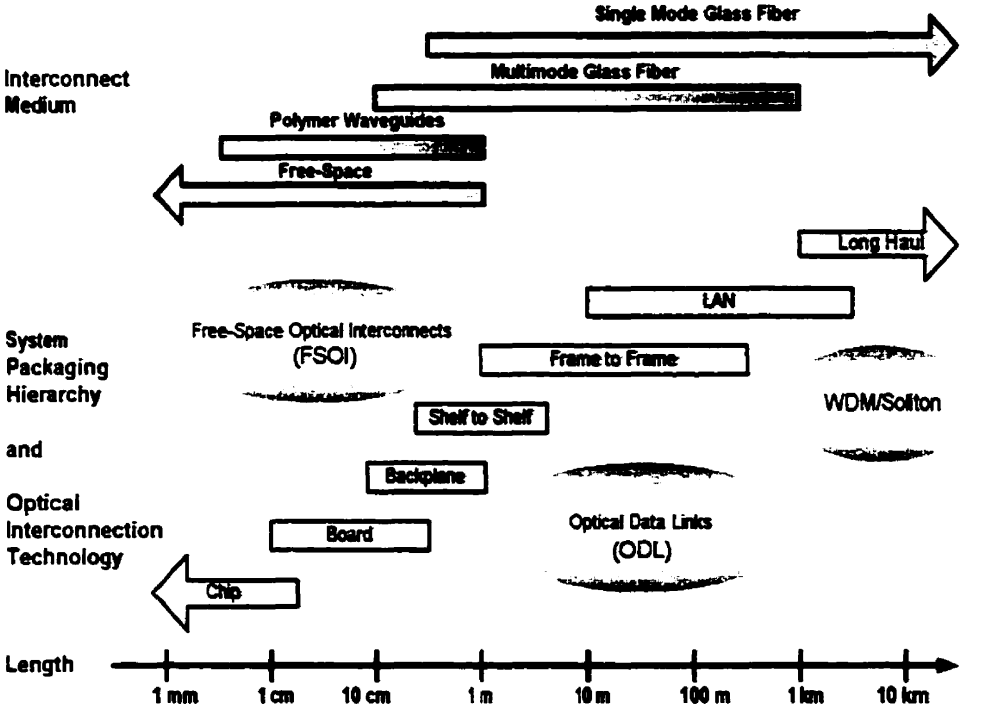

Figure 1.1. Conventional digital system interconnection hierarchy and technology

1.1.1 Limitations of Electrical Interconnections

At very high data rates, difficulties arise when moving digital information off-chip i.e. interconnection traces behave more like transmission lines and packaging density restrictions become more severe. At 500 Mbits/s in standard 50 Ω twinex cables, a

transmission length is limited to less than 10 meters due to difficulties associated with attenuation and compliance with electromagnetic interference (EMI) standards [5]. Physical limitations of electrical interconnections in high-speed digital electronic system include [6]:

- High power dissipation from line drivers due to capacitive loading effects.
- Signal distortion due to reflections from improperly terminated lines.
- Capacitive and inductive crosstalk, signal dispersion, switching noise, and reflections also contribute to signal distortion at high frequencies.
- Greater attenuation at high frequencies due to the skin effect.
- Sensitivity to EMI and grounding voltage interference.
- Skew resulting from delay variations.

These limitations combined with predictions from the semiconductor technology roadmap in which the demand for integrated circuits (ICs) I/O is expected to grow exponentially and combined with the cost of implementing high-speed electrical interconnects has significantly stimulated research into alternative technologies.

1.1.2 Benefits and Trade-Offs of Optical Interconnections

With increasing data rates, transmission lengths, and I/O density, electrical limitations become even more apparent. The potential benefits of optical interconnections may resolve most of the physical restrictions incurred by their counterparts [4]. At the moment, the cost of implementing short to medium distance optical links is still high and optical links themselves pose several technological challenges. The primary limitations of optical interconnects are [6]:

- Alignment and packaging of optical transmitters, optical channel elements, and optical receivers.
- Active or passive optoelectronic transmitter and receiver cost, reliability and fabrication issues.

- Optical power attenuation along interconnection path.
- Delay of signals, although relatively constant across parallel channels, is less than for electrical connections due to longer physical path lengths.
- Eye safety and cost of optical interconnects.

As speeds and densities of modern computers and communication systems continue to increase, a point will be reached were the trade-offs between electrical and optical interconnections will begin to favor optical solutions.

1.2 Choice of Transmitter Technology

Several optoelectronic technologies for parallel optical interconnections are currently available, they include multiple quantum well (MQW) modulators and semiconductor laser arrays. Electro-absorption modulators hybridized (flip-chip) to CMOS integrated circuits and modulating continuous wave (CW) laser beams have become an accepted choice for free-space optical interconnects (FPOI) [7-8]. Modulators appear to be an excellent transmitter choice from power dissipation, fabrication and reliability considerations. However the primary disadvantage of modulator based approaches is the additional system complexity caused by the external power supply.

Worldwide advances in semiconductor laser diodes over the past few years have led to the emergence of Vertical-Cavity Surface Emitting Lasers (VCSELs) which are quickly becoming a promising low cost optical emitter technology. Optical beams propagating in a system can be directly produced and modulated from a VCSEL array. For optical applications they offer several advantages such as wafer-level testing, circular output beams, compatibility with flip-chip bonding and easy fabrication of two-dimensional arrays. The lasing cavity in VCSELs is very small so that device speeds are very high and threshold currents for lasing action are very low, reducing both waste heat and the complexity of driving circuitry. Methods of integrating III-V semiconductor VCSELs with Si integrated circuits are being developed and their potential has been demonstrated in many parallel data links.

1.3 Parallel Optical Data Links (PODLs)

In recent years, the development of parallel optical data links has advanced rapidly. They can be used for physically parallel, functionally serial high bandwidth links such as intershelf and intercabinet interconnections or in physically and functionally parallel applications such as CPU to remote memory and/or memory bus [9]. They are being developed for relatively short distances: typically from half a meter to a few hundred meters with per-channel throughputs ranging from 200 to 1000 Mbit/s.

With the overall performance improvements of VCSELs, several optical data links have been demonstrated. Among notable ones are the parallel link projects by the Opto-electronic Technology Consortium (OETC) [10], by the Parallel Optical Link Organisation (POLO) [5], the Optobus project by Motorola Corp. [11] and more recently the ParaBIT project by NTT Corp. [12]. The success of these projects has led to the development of one-dimensional commercial links currently available from several companies [13-14]. Table 1.1 summarises VCSEL based fiber ribbon PODLs and their performances. Several other projects based on edge-emitting lasers have also been reported with comparable performances to the data links listed in table 1.1 [15-16]. Current commercial links are compatible with most standards, such as fiber channel, IEEE 802.3z Gigabit Ethernet (GbE), HiPPI 6400 and ATM [14].

	OETC	POLO	Optobus	ParaBIT	Siemens	Mitel
Year	1994	1995	1995	1999	1998	1999
Capacity	16 Gbit/s	8 Gbit/s	2 Gbit/s	28 Gbit/s	15 Gbit/s	24 Gbit/s
Gbit/s ch.	0.5	1	0.2	0.7	1.25	2
# of ch.	32	10	10	40	12	12
Distance	100 m	300 m	30 m	--	75 m	--
Detector	MSM	PIN	PIN	PD	PIN	PIN

Table 1.1. VCSEL based PODLs

Module integration and packaging is a key issue in realizing practical interconnections. A typical ODL module is shown in Figure 1.2. Most, if not all (detailed information is not available for the commercial links) of the VCSEL based links, use intermediate

components such as 45°- mirror polished fibers or waveguides between the VCSELs and the fiber connectors. Further, their one-dimensional configurations require active or visual alignment of the VCSELs to the package.

Linear fiber ribbons used in most PODLs do not scale well into two dimensions. The spatial advantage of two-dimensional arrays of optolectronic - very large scale integrated (OE-VLSI) circuits is not fully utilized nor is the cost advantage of passive alignment. For these reason faster, simpler and cheaper 2D VCSEL integration and packaging is required [17]. 2D optical data transmission has been achieved with a variety of optical media, including free-space optics [18-19], 2D arrays of optical fibers [20], and optical fiber image guides (FIGs) [21].

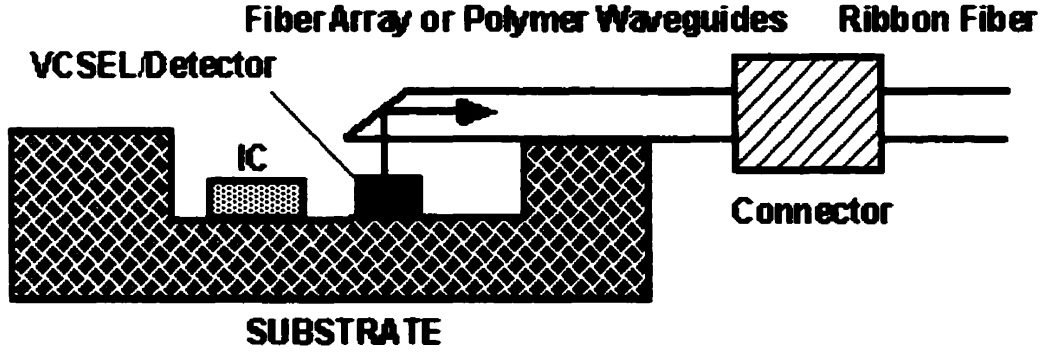

Figure 1.2. VCSEL based one-dimensional parallel link module

Free-space optical interconnections may have applications for short distance (1 m or less) multiple channel interconnects and are also employed for long distance single channel interconnects, but are not suitable for multiple channel long-distance interconnect applications due to diffraction-induced beam-spreading and the difficulty of maintaining alignment accuracy. Ordered arrays of optical fibers (with one fiber per transmitter-receiver pair) are potentially useful but present significant challenges of fabrication. The remaining alternative which can be suitably fitted for point-to-point interconnections is the optical fiber image guide. In short distance applications however, such as board-to-board, there is insufficient separation between boards (less than 25 mm) to allow the use of fiber bundles or image guides [22].

1.4 Benefits of Fiber Image Guides (FIGs)

Interconnections using one fiber per channel require individual alignment of each fiber to each transmitter and receiver. The use of a fiber image guides consisting of a bundle of many thousand equally spaced fibers relaxes alignment tolerances and ensures that one or more channels can be damaged without the loss of all power in a channel. Several methods have been demonstrated to couple light including the use of micro-lens arrays, bulk lenses, taper based coupling and butt-coupling.

1.5 Project Overview

In order to evaluate and demonstrate the suitability of 2D optical interconnects based on VCSELs and fiber image guides several issues must be addressed. These include techniques to align light emitted from the far end of the image guide to a detector array (many demonstrations to-date have employed single channel detectors or CCD cameras), the level of signal uniformity across channels, the total loss in the system and the level of optical crosstalk. This thesis is a detailed elaboration of a manuscript submitted to Applied Optics [23] in which these issues have been addressed by demonstrating the parallel transmission of optical signals from an 8X8 VCSEL array through a 1.35 m long image guide. These signals were successfully optically aligned to metal-semiconductor-metal (MSM) receiver array with a compact modular optical system as shown in Figure 1.3. In addition to presenting experimental results of optical data rates, loss and crosstalk, image guide specific properties such as bandwidth and throughput uniformity determined by the optical spot size were also investigated.

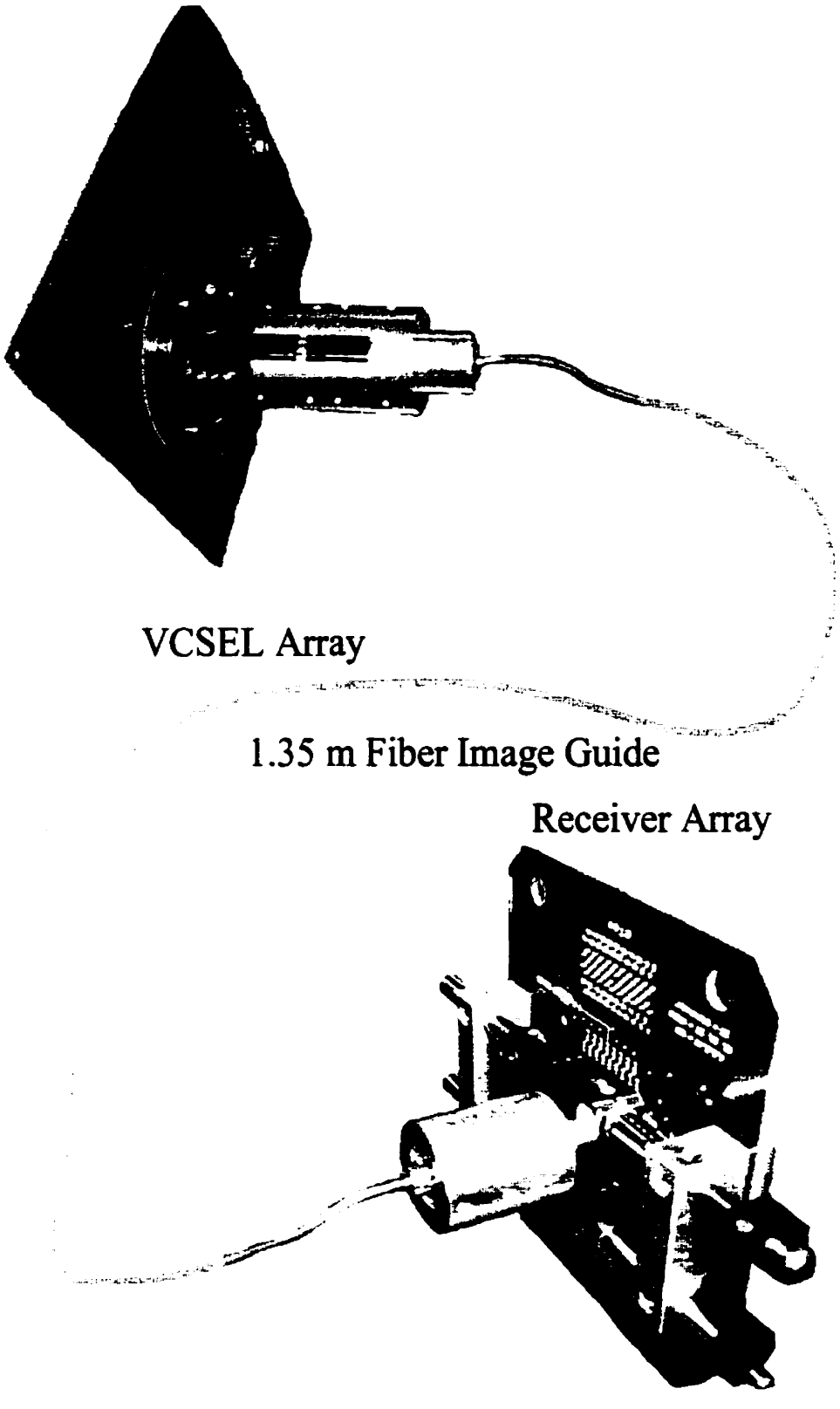

Figure 1.3. Image guide based parallel optical link demonstration [21]

1.6 Thesis Outline

Following an introduction to the concept and emergence of VCSEL based optical data links as well as the motivation for two-dimensional links, the subsequent chapters are organized as follows. Chapter 2 presents the fundamentals of active optoelectronic devices such as semiconductor lasers and receivers while addressing the properties of the available components for the assembly of the FIG based interconnect. In chapter 3, fiber image guide technology is described in great detail with its limitations and advantages. Image guide throughput uniformity and other significant characteristics will also be presented. This leads to a description in chapter 4 of the design and construction of the FIG based bit-parallel optical data link. The characterization and performance limitations of the system are discussed in chapter 5. To conclude, chapter 6 summarises the obtained results and suggests system requirements and directions for future FIG development.

1.7 References

1. Y. Li, T. Wang, H. Kosaka, S. Kawai, and K. Kasahara, "Fiber-image-guide-based bit-parallel optical interconnects," Appl. Opt. 35, 6920-6933 (1996).

2. K. Emura, "Ultra-Large Capacity WDM Transmission Technology", *in The Sixth Microoptics Conference and the Fourtheenth Topical Meeting on Gradeint Index Optical Systems.* MOC/GRIN Technical Digest (The Japan Society of Applied Physics, Tokyo, 1997), pp.324-327, 1997.

3. J.E. Medwinter, Photonics in switching, Volume 1, Background and Components, Academic Press, Inc., Boston, pp. 1-16, 1993.

4. R.A. Nordin, A.F.J. Levi, R.N. Nottenburg, J. O'Gorman, T. Tanbun-Ek, and R.A. Logan, " A System Perspective on Digital Interconnection Technology", *Jour. of Lightwave Tech.*, vol. 10, no. 6, pp. 811-827, June 1992.

5. W.S. Ishak, K.H. Hahn, B.L. Booth, C. Muheller, A.A.J. Levi, and R. Craig, "Optical interconnects: The POLO project." in *Optoelectronic interconnects III,* R. T. Chen and H. S. Hinton, eds., Proc. SPIE 2400, 214-221 (1995).

6. F.B. McCormick, in Photonics in Switching, Volume II, Systems, edited by J.E. Midwinter, Academic Press, Inc., Boston, pp. 169-250, 1993.

7. D.V. Plant, A.Z. Shang, M.R. Otazo, D.R. Rolston, B. Robertson, and H.S. Hinton, "Design, Modeling, and Charaterization of FET-SEED Smart Pixel Transceiver Arrays for Optical Backplanes", *IEEE Jour. Quant. Elec.*, vol. 32, no. 8, pp. 1391-1398, August 1996.

8. H.S. Hinton, T.J. Cloonan, F.B. McCormick, A.L. Lentine, and F.A.P. Tooley, "Free Space Digital Optical Systems", *Proc. of the IEEE*, vol. 82, no. 11, pp.1632-1649, 1994.

9. J.D. Montgomery, and S. Montgomery, "Parallel optical links fill integrated-circuit niches", Laser Focus World 35(4), 57-59 (1999).

10. Y.M. Wong, D.J. Muehler, C.C. Faudskar, D.B. Buchholz, M. Fishteyn, J.L. Brandner, W.J. Parzygnat, R.A. Morgan, T. Mullally, R.E. Leibenguth, G.D. Guth, M.W. Facht, K.G. Glogovsky, J.L. Zilko, J.V. Gates, P.J. Anthony, B.H. Tyrone, T.J. Ireland, D.H. Lewis, D.F. Smith, S.F. Nati, D.K. Lewis, D.L. Rogers, H.A. Aispain, S.M. Gowda, S.F. Walker, Y.H. Kwark, R.J.S. Bates, D.M. Kuchta, and J.D. Crow, "Technology development of high density 32-channel 16 Gb/s Optical Data Link for Optical Interconnection Applications for the Optoelectronics Technology Consortium (OETC)", Journal of Lightwave. Tech. 13(6), 995-1016 (1995).

11. D.B. Schwartz, C.K.Y. Chun, B.M. Foley, D.H. Hartman, M. Lebby, H.C. Shieh, S.M. Kuo, S.G. Shook, B. Webb., "Optobus: A low cost, high performance optical interconnect," *Technical Digest of 45th Electronic Components & Technology Conference (ECTC '95)*, pp. 376-379, May 1995.

12. K. Katsura, Y. Ando, M. Usui, A. Ohki, N. Sato, N. Matsuura, N. Tanaka, T. Kagawa, and M. Hikita, "ParaBIT: Parallel Optical Interconnection for Large-Capacity ATM Switching Systems", *IEICE Trans. Commun.*, vol. E82-B, no. 2, Feb. 1999.

13. 12L485 VCSEL array and 12L486 PIN array from Mitel Semicondutors, Data sheet.

14. Parallel Optical Links - PAROLI Family, Infineon Technologies (Siemens Corp.), Data sheet.

15. R. Nagarajan, W. Sha, B. Li, and R. Craig, "Gigabyte/s Parallel Fiber-Optic Links Based on Edge Emitting Laser Diode Arrays", *J. of Lightwave Tech.*, vol. 16, no. 5, pp. 778-787, May 1998.

16. H. Karstensen, C. Hanke, M. Honsberg, J.R. Kropp, J. Weiland, M. Blaser, P. Weger, and J. Popp, "Parallel Optical Interconnection for Unencoded Data Transmission 1 Gb/s-per-channel capacity", *J. Lightwave Technol.*, vol. 13, pp. 1017-1030, 1995.

17. H. Kosaka, "Smart Integration and Packaging of 2-D VCSEL's for High-Speed parallel Links", *IEEE J. of Selected Topics in Quant. Elect.*, vol. 5, no. 2, pp.184-192, 1999.

18. D.V. Plant, B. Robertson, H.S. Hinton, M.H. Ayliffe, G.C. Boisset, W. Hsiao, D. Kabal, N.H. Kim, Y.S. Liu, M.R. Otazo, D. Pavlasek, A.Z. Shang, J. Simons, K. Song, D.A. Thompson, and W.M. Robertson, "4X4 vertical-cavity surface-emitting laser (VCSEL) and metal-semiconductor-metal (MSM) optical backplane demonstrator system," Appl. Opt. 35, 6365-6368 (1996).

19. D.J. Goodwill, "Free space optical interconnect for terabit network elements", *in Optics in Computing, OSA Technical Digest* (Optical Society of America, Washington, DC, 1999), pp. 208-210, 1999.

20. A.G. Kirk, F. Mathieu, D. Plant, M. Mony, P. Khurana, C. Cryan, K. Tateno, and T. Kurokawa, " Two-Dimensional Optical Interconnects with Fiber Arrays", in *The Sixth Microoptics Conference and the Fourteenth Topical Meeting on Gradient Index Optical Systems*, MOC/GRIN Technical Digest (The Japan Society of Applied Physics, Tokyo, 1997), pp. 296-299, 1997.

21. T. Maj, A. Kirk, D. Plant, J. Ahadian, C. Fonstad, K. Lear, K. Tatah, M. Robinson, J. A. Trezza, 'Interconnection of a 2D VCSEL array to a receiver array via a fiber image guide', *in Optics in Computing, OSA Technical Digest* (Optical Society of America, Washington, DC, 1999), PD2.

22. F.A. Tooley, "Challenges in Optically Interconnecting Electronics", *IEEE J. of Selected Topic in Quant. Elec.*, vol. 2, no. 1, pp. 3-13, April 1996.

23. T. Maj, A. Kirk, D. Plant, J. Ahadian, C. Fonstad, K. Lear, K. Tatah, M. Robinson, J. A. Trezza, 'Interconnection of a two-dimensional VCSEL array to a receiver array via a fiber image guide', *Applied Optics*, to be published, April 2000.

Chapter 2

Active Optoelectronic Devices

2.1 Introduction

Devices which are able to convert electrical-to-optical signals and vice-versa are crucial components for the realization of any optical interconnection. For single channel systems optical-to-electrical detectors and receivers are more developed than transmitters. Many research groups have therefore focused their energies on making vertical-cavity surface-emitting lasers (VCSELs) a high performance transmission source for optical communication. With exceptional electrical and optical properties, these devices are quickly achieving a market acceptance. The largest application for laser diodes is in CD pick-up heads and many companies are now considering to use VCSELs in their CD players. Other applications that could benefit from these advancements include high-speed opto-couplers, laser printers, laser pointers, sensors, bar-code scanners, displays, optical encoders as well as efficient pump sources for solid-state lasers.

This chapter begins with an overview of VCSEL structures, properties and performances along with an emphasis on design characteristics for an 8X8 VCSEL array used in the implementation of the optical link presented in chapter 4. In section 2.3, beam propagation models and optical properties of the VCSEL array will be presented and finally in section 2.4, receiver fundamentals will also be reviewed and a receiver array will be introduced.

2.2 Optoelectronic Transmitter Technology

Semiconductor lasers have been a subject of research in laboratories around the world for three decades; the first room temperature semiconductor laser has been demonstrated in 1973 [1]. VCSELs are a particular type of semiconductor diode laser, which is becoming

increasingly more important. After a decade of research, VCSELs have evolved from initial laboratory curiosities to prototype lasers exhibiting record efficiencies to a manufacturable optoelectronic technology being pursued by many companies. The following sections will provide an overview of VCSELs structures. VCSEL characteristics with respect to an 8X8 proton implanted array will be described in detail and principles of high-speed operation will also be surveyed.

2.2.1 VCSEL Structures

VCSELs are built in a stack of layers of different material composition. Feedback is enabled through the use of distributed Bragg reflector (DBR) mirrors to form the laser cavity as opposed to cleaving or dry etching for conventional edge emitting lasers. DBRs are alternating pairs of semiconductor crystal that provide reflectivity of 99.9% or higher [2]. This structure enables VCSEL emission to be perpendicular to the wafer surface and a typical proton implanted VCSEL is shown in Figure 2.1. The main components are two high-reflectivity DBR mirrors separated by a thickness of a multiple of $\lambda/2$ to form a high finesse Fabry-Perot cavity [3]. The gain medium is located between the mirrors. It is commonly composed of one or more very thin semiconductor layers to form the quantum wells. The material selected for the quantum wells determines the wavelength regime. Therefore GaAs is the material of choice for VCSELs operating in the 850 nm regime.

Current confinement across the gain region is established through a proton-implanted aperture [4]. This structure is very simple to manufacture and most commercial VCSELs are based on this technology. However, this structure lacks current confinement and current research is focused on oxide-confined structures. The oxide-confined approach simultaneously increases current injection efficiency and reduces series resistance, thus leading to a major improvement of power conversion efficiency. Impressive results, such as threshold currents below 40 μA [5], and wall plug efficiencies above 50% [6], have been achieved. Reliability studies for oxide-confined VCSELs are currently being undertaken; it is anticipated that they will soon be out of the labs and into production [7].

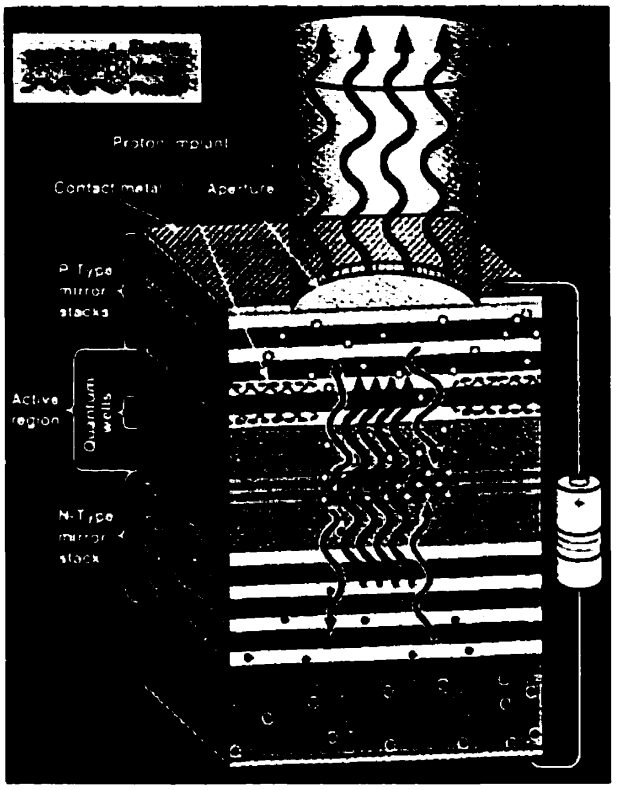

Figure 2.1. Proton implanted VCSEL structure

VCSELs thin active layers and mirror layers are usually deposited onto GaAs substrates using growth techniques such as molecular beam epitaxy (MBE) and metal organic chemical vapor deposition (MOCVD). The advancement of these growth technologies played a major role in VCSEL development. VCSELs consequently offers many advantages compared to traditional edge emitting lasers:

1. A circular laser beam with a low numerical aperture (NA).
2. The requirement of only standard batch fabrication processes used in silicon integrated circuit fabrication.
3. The ability of wafer-level testing before packaging.
4. The capability of fabricating dense two-dimensional arrays (32 X 32 arrays have been demonstrated).
5. Compatibility with flip-chip bonding techniques.
6. Can be directly modulated from a NRZ data stream with fixed bias and drive currents.

Some of these inherent advantages will enable high-volume and low cost VCSEL manufacturing. It is also predicted that improvements in manufacturing will result in single transverse mode, high efficiency, low threshold (< 300 μA) and low operating voltage (< 2 V) VCSELs which are compatible with simple driver circuits [8-10].

2.2.2 VCSEL Characteristics

Figure 2.2 shows a top view of a VCSEL array. For VCSELs, as well as for other lasers, LI curves are a key parameter for their characterization. An LI curve is a plot of Light intensity (optical power) vs Injected current into a laser. A VI curve or Voltage vs Injected current is another important parameter which helps to determine the DC characteristic impedance of a diode. Figure 2.3 shows measured LIV curves for randomly selected VCSELs on the 8X8 array obtained form MicroOptical Devices, Inc. The threshold current, I_{TH}, from the 15 μm diameter VCSEL aperture seems to vary by more than 10% across the array. LI curves for one-dimensional arrays have been reported with less variation across a 10 VCSEL array [11].

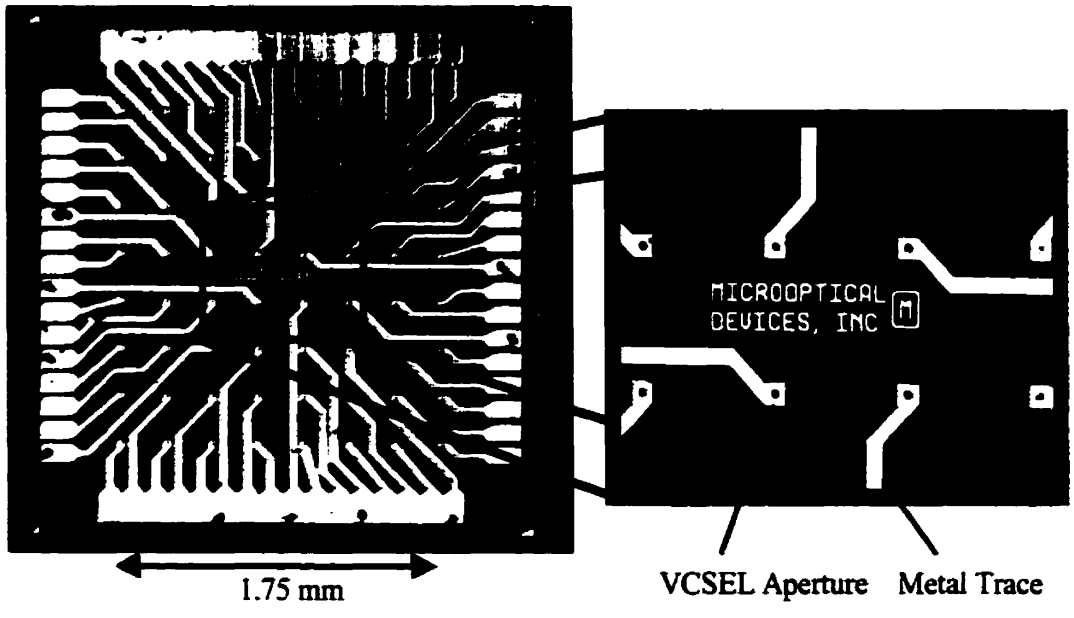

Figure 2.2. Top view of an 8X8 VCSEL array

Since the length of the optical cavity in a VCSEL is very short, only one wavelength will overlap with the laser gain bandwidth. Thus, a single longitudinal optical mode is an inherent VCSEL characteristic. Furthermore, the lasing wavelength in a VCSEL is determined by the Fabry-Perot resonance defined by its distributed Bragg reflector (DBR) mirrors. Because the gain peak of the quantum well emission and the resonance of the DBR mirrors change at different rates with temperature, the VCSEL I_{TH} (threshold current) is a minimum at a temperature where the peak of the quantum well emission coincides with the DBR resonance. Because of this, the cavity resonance is often intentionally designed to be at slightly longer wavelength relative to the peak laser gain at room temperature, so that at higher operating temperatures, the peak laser gain shifts into alignment with the cavity resonance to yield optimum VCSEL performance [12].

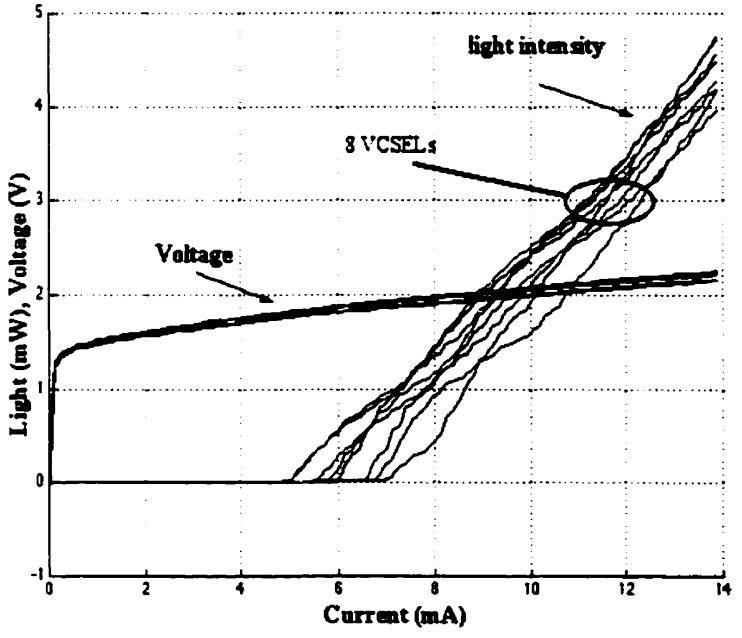

Figure 2.3. LIV curves for several VCSELs

VCSEL behavior with respect to temperature has a direct impact on LIV characteristics. Several readings were performed on a VCSEL from the 8X8 VCSEL array and Figure 2.4 shows typical LIV curves with respect to temperature. Clearly the minimum I_{TH} is achieved around 41-48°C. As expected, increasing the temperature from room

temperature will decrease the threshold current. Slope efficiency or the efficiency of a laser in converting electrical power into optical power is normally difficult to predict since it depends on several parameters such as material absorption, mirror reflectance, laser gain, etc. In general, slope efficiency decreases approximately linearly with temperature. This is also shown by the curves in Figure 2.4.

For semiconductor diodes, the junction voltage at a fixed current decreases as the temperature increases. The VCSEL is no exception and the IV curves from Figure 2.4 confirm the behavior. Basically the effective resistance decreases as the temperature increases. In driver circuit design, the series resistance should not be ignored since it is typically above 20 ohms.

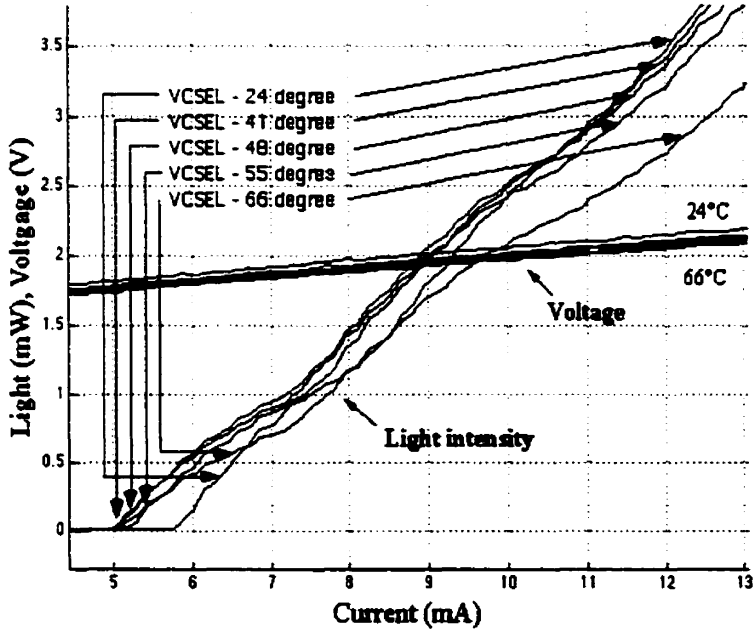

Figure 2.4. VCSEL LIV characteristics versus temperature

All lasers exhibit a relaxation resonance, which produces oscillation on the pulse rising edge. If this oscillation is too near the operating frequency or too large a magnitude, it can severely limit laser performance. In VCSELs relaxation resonance is typically above 5 GHz and can be ignored for Gigabit applications. Turn-on delay however, is a serious

issue. If a low state or bit is represented by an optical power below the threshold current, the rising edge delay might become unacceptably large. Because this effect does not occur on the falling edge, the result is pulse distortion. Also, when a pulse goes from a high level to a low level, there is a rapid decay drop. At higher data rates, it may take more time for the last few percent to decay away and if a pulse is preceded by multiple zeros, it will behave as if it rose directly from zero. However, if it is preceded by multiple ones and a single zero, the rising edge begins from a level above true zero. This results in data dependent jitter on the rising edge, which is demonstrated in Figure 2.5 on a VCSEL from the 8X8 array. The rising edge is delayed by approximately 2 ns, thus for data rates above 250 Mbit/s proper biasing must be set on all VCSELs.

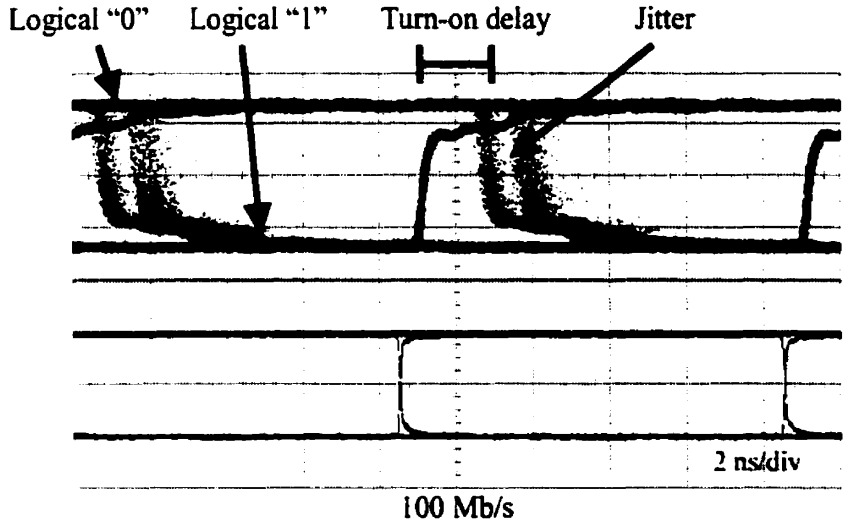

Figure 2.5. VCSEL turn-on delay (bottom trace is the electrical input signal)

2.2.3 *VCSEL High-Speed Modulation*

In order to achieve an optimum performance from a VCSEL based transmitter it is important to understand its modulation characteristics. High modulation speeds of 1 Gbit/s have been achieved without any biasing [13]. In general, for commercial proton implanted VCSELs, to properly balance the design of extinction ratio and turn-on delay jitter, it is necessary to bias the VCSEL above the threshold, typically with less than 0.5 mA difference between I_{BIAS} and I_{TH} [14]. This is complicated by the variation of the

VCSEL threshold current over temperature. Therefore it is important to actively control the temperature of the VCSEL during operation. Operating the VCSEL at a higher bias current will result in a higher average power dissipation.

Small modulation currents, less than 4 mA, result in poor performance. The sensitivity to temperature and lifetime degradation is enhanced when a small change in threshold current is a large fraction of the modulation current. High-speed modulation also requires higher modulation currents. The efficiency of the complete optical system (VCSEL, optics, optomechanics, etc.) determines the required modulation current. It is usually not acceptable to lower the effective efficiency by intentionally misaligning or defocusing to decrease coupling. Such schemes might lead to anomalous optical waveforms.

Impedance matching is very important when designing high-speed systems. The series resistance of a VCSEL must be taken into account. The VCSEL driver must be designed for a particular impedence, whether directly attached or at the end of a transmission line. Anomalous waveforms can result if the VCSEL, line and driver are not matched. Other factors influence the matching of a system, but is it usually recommended to aim for no worse than a 10% mismatch [14].

For experimental purposes, the simplest VCSEL modulation scheme is to use a bias tee with the DC port connected to a bias current and the AC port directly connected to a pulse generator [15]. Care must be taken to carefully control the voltage swing because a function generator is not current limited and will not protect the VCSEL from current surges. An alternative is to use a high-speed commercial laser diode driver with direct access to laser modulation and biasing. None of the two previous schemes are convenient for driving VCSEL arrays since they will require too much space and too many components for a practical system. Current approaches design application-specific integrated circuits (ASICs) which offer the convenience to drive an entire arrays. Such an ASIC can easily be packaged beside a one-dimensional VCSEL array [16] or recently with more efficient packaging, a 16X16 VCSEL array was hybridized (flip-chip) to a CMOS VLSI driver circuit [17].

2.3 VCSEL Optical Characteristics

In order to properly design an optical system, laser beam characteristics must be well understood. Single transverse mode operation increases the efficiency of coupling light into fiber optic cables, and the low longitudinal mode count significantly reduces chromatic dispersion in a fiber. In VCSEL emission, the output is typically multi-transverse and single longitudinal with a typical spectral width less than 5 Angstroms, which ensures a low coherence source [18]. The symmetric circularity and non-astigmatic emission from a VCSEL is usually maintained even with multi-transverse modes.

2.3.1 Gaussian Beams

Optical system modeling via ray tracing is often simple and satisfactory but it has its limitations. A ray represents a path; it is not a field nor does it have an amplitude nor a phase. Consequently it is necessary to obtain a more complete wave description of the beams produced by a laser. A Gaussian beam propagation model is often used in design calculations for optical systems [19] and the fundamental mode of a VCSEL is Gaussian or very close to it [20].

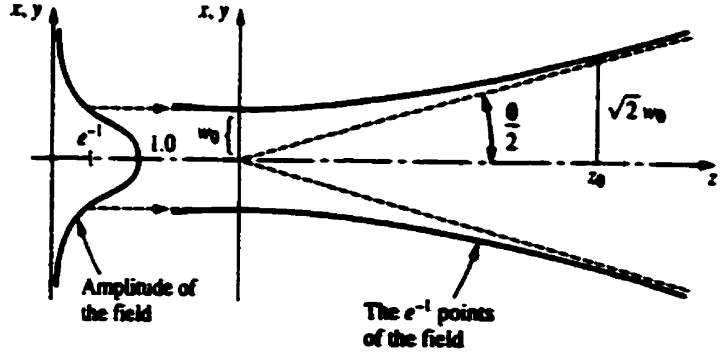

Figure 2.6. Propagation of the $TEM_{0,0}$ mode [21]

Figure 2.6 shows a typical beam spreading illustration for a single transverse or lateral mode source. Within any transverse plane, the beam intensity assumes its peak value on

the beam axis, and drops by a factor of $1/e^2 \sim 0.135$ at the radial distance W(z). Since 86% of the power is carried within a circle of radius W(z), W(z) is called beam radius or beam width. A field is well approximated by the following Gaussian beam propagation equation [21]:

$$W(z) = W_o \left[1 + \left(\frac{z}{z_o} \right)^2 \right]^{\frac{1}{2}} \qquad \text{Equation 2.1}$$

Where:

$$z_o = \frac{W_o^2 \pi}{\lambda} \text{ is the Rayleigh range.}$$

W_o is called the beam waist and assumes its minimum value in the plane $z = 0$. The beam diameter 2W(z) is often specified as spot size or mode field diameter (MFD). As the beam propagates ($z >> z_o$), its radius increases approximately linearly with z. The angular divergence θ is often approximated by the following relationship:

$$W(z>>z_o) = W_o \frac{z}{z_o} = \frac{z\lambda}{\pi W_o} \qquad \text{Equation 2.2}$$

$$\theta/2 = \frac{dW}{dz} = \frac{\lambda}{\pi W_o} \qquad \text{Equation 2.3}$$

$$\theta = \frac{2\lambda}{\pi W_o} \qquad \text{Equation 2.4}$$

Several VCSEL manufactures specify their product with a divergence angle that corresponds to a Full Width Half Maximum (FWHM). This refers to the full divergence angle measured at half the maximum power points.

Multi transverse mode structures, however, are more difficult to predict and model. Higher order mode components produce a larger divergence than a single-mode beam. To

account for these higher modes an alternate model has been developed. It is based on a constant, M^2, derived from the uncertainty principle and can be measured to characterise mixed-mode beams [22]. Figure 2.7 shows an imbedded Gaussian in a construct for deriving multimode beam parameters. A higher mode that has a waist M times larger than the waist of the imbedded Gaussian will have a beam M time larger everywhere. Equation 2.1 and 2.4 can be modified to account for the M^2 parameter [22]:

$$W_M = W_{oM}\left[1+\left(\frac{M^2 z\lambda}{\pi W_{oM}^2}\right)^2\right]^{\frac{1}{2}} \qquad \text{Equation 2.5}$$

$$\Phi = M\,\theta = M^2\left(\frac{2\lambda}{\pi W_{oM}}\right) \qquad \text{Equation 2.6}$$

Where:

W_{oM} is the multimode waist.

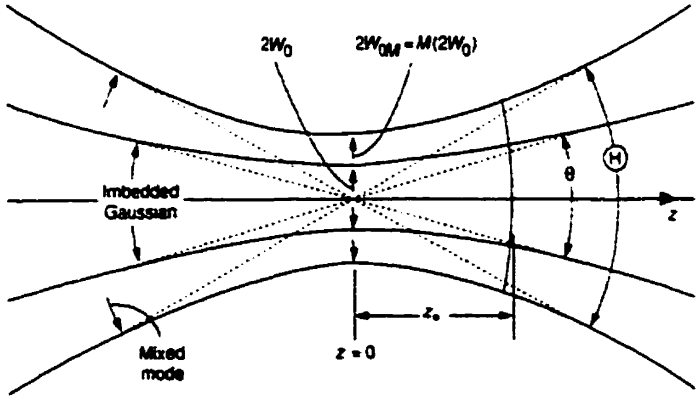

Figure 2.7. Imbedded Gaussian model [22]

2.3.2 VCSEL Transverse Mode Characteristics

From the specifications, the 8X8 VCSEL array used in this research is a multi-transverse mode source. Several modes other than the fundamental $TEM_{0,0}$ mode can be stimulated at the same time [23]. Using a one-dimensional beam scanner, Beam Scan by Photon

Inc., far-field mode profiles for different injected currents were obtained as shown in Figure 2.8. At a low injected current i.e. slightly above threshold the profile of the beam from the VCSEL array behaves very close to an ideal Gaussian beam i.e. there is a 98% fit. However, as the injected current is increased, additional lateral modes appear and as shown in Figure 2.8 (b) the profile of the beam takes on a donut shape.

The angle of divergence is also affected by the injected current. With an injected current of 8 mA, the full divergence angle is approximately 18 degrees; with a current of 18 mA, the divergence angle increases to 24 degrees. By following the test procedure suggested by the Beam Scan software an M^2 factor of 3.3 ± 10% at 10 mA was measured.

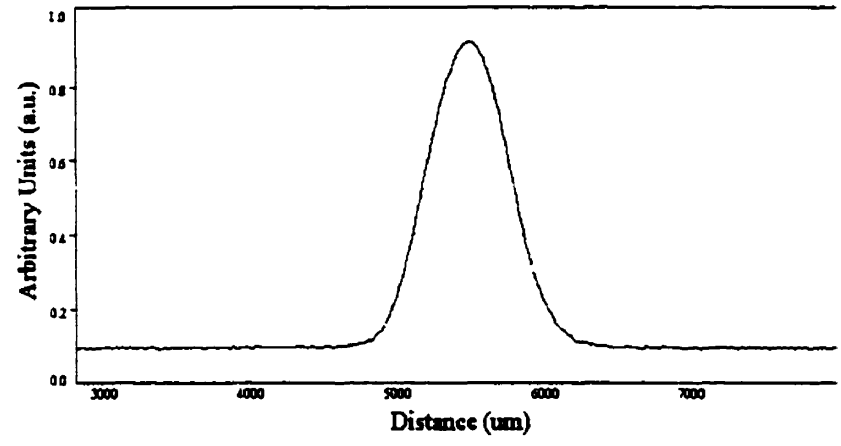

(a) I= 9 mA

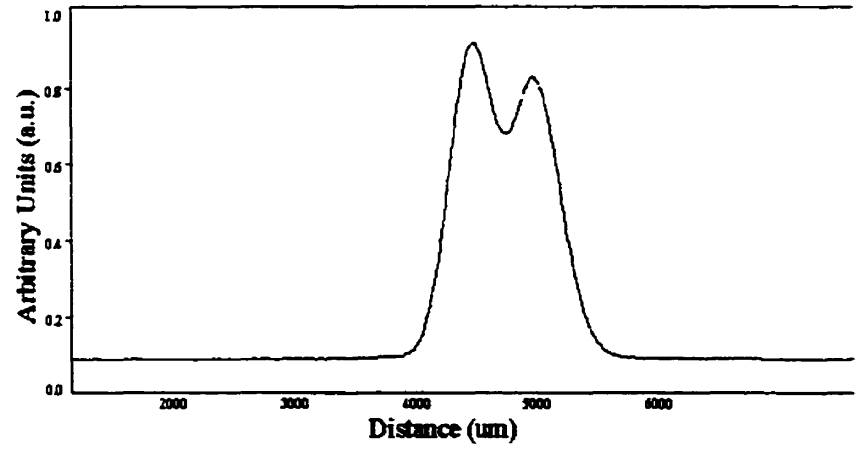

(b) I = 15 mA

Figure 2.8. VCSEL one dimensional far-field beam profiles

2.4 Receiver

A receiver is an integral part of any optical communication system, its function is to convert optical signals into electrical ones. A 4X4 receiver array used in the fiber image guide system presented in chapter 4 is a typical example. The following sections will outline the fundamental concepts behind receiver design and will briefly describe and characterise the receiver array.

2.4.1 Receiver Fundamentals

A detector in an optical data link is typically a diode structure. When a photon with energy greater than the bandgap of the semiconductor material enters the device, it is likely to be absorbed. If the device is biased appropriately a current will be produced. Typical photodetector structures are photodiodes (pn junction), p-i-n diodes and avalanche photodiodes (APD). Photodetectors are described by their responsivity, noise characteristics, and spectral response characteristics.

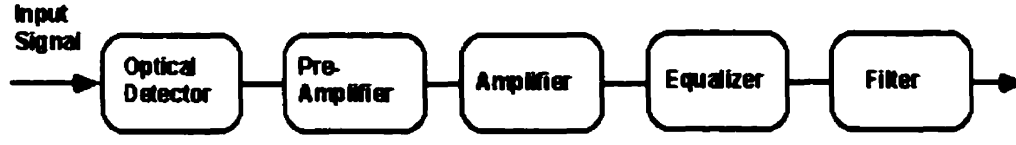

Figure 2.9. System representation of an O-E receiver

A block schematic of a typical optical fiber receiver is shown in Figure 2.9. Since a photodetector usually has high output impedance it is most efficient when driving a low impedence input. Therefore a transimpedance amplifier usually follows an optical detector. Initial amplification can also be performed with a preamplifier circuit where it is essential that additional noise is kept to a minimum. An equalizer is often included in a receiver to compensate for any distortion from the amplifier or to provide a suitable signal for the filter. Finally, the function of the filter is to maximize the signal to noise ratio while preserving essential features of the signal [24].

2.4.2 4X4 Receiver Array

For the project we used a fully differential receiver which was designed at the Massachusetts Institute of Technology (MIT) and fabricated by the Vitesse GaAs process [25]. The array was designed to provide a greater noise immunity and to eliminate line drivers. The receiver is a monolithic GaAs integrated circuit which combines a 4X4 photodetector array on a 250 μm pitch, 1 Gbit/s transimpedance amplifier, and ECL output drivers [25]. Figure 2.10 illustrates the schematic of the differential circuit. The first-stage transimpedance amplifier and second-stage voltage amplifier are followed by the cascade of a transconductance and a transimpedance amplifier [25].

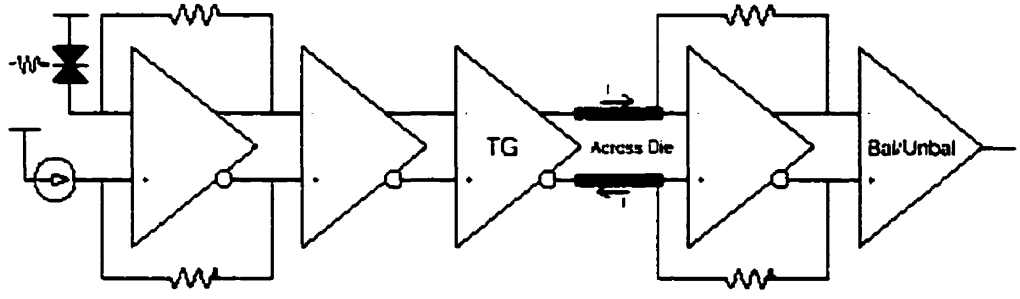

Figure 2.10. Block representation of differential optical receiver [25]

The photodetector array is based on 75 μm diameter metal-seminconductor-metal (MSM) photodetectors with 2.1 μm finger spacing. A photograph of the MSM diode is shown in Figure 2.11. The MSM diode has several advantages over standard photodiodes. First, because the structure is planar, the fabrication is simple and leads to high yields. The parasitic capacitances between contacts are much smaller than for vertical diodes of the same active area. The net effect is to reduce the overall capacitance, leading to fast devices [26]. Speed is further increased by the spacing between the fingers being smaller than for vertical diodes, giving short carrier transit times. The MSM photodetectors on the array require a 15-35 μW optical input swing to perform a bit transition. Figure 2.12 shows the layout of the 2.3 mm X 2.3 mm die.

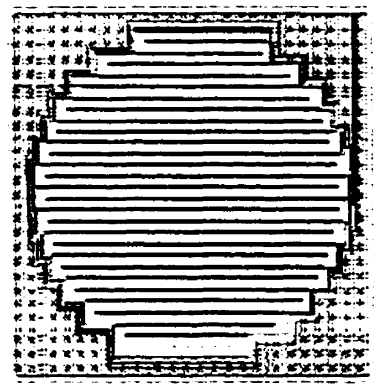

Figure 2.11. Layout of MSM photodetector [24]

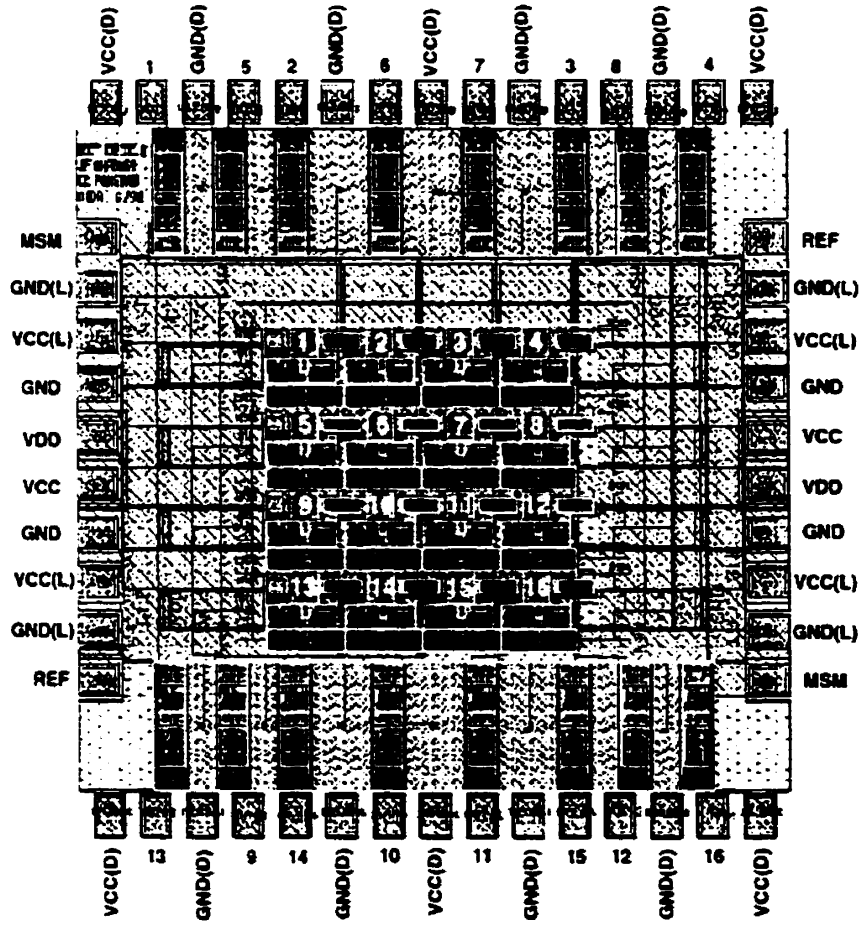

Figure 2.12. Layout of optical receiver [24]

2.5 Conclusion

In this chapter active optoelectronic devices were introduced along with an emphasis on VCSEL arrays and MSM based receivers. From a system integration perspective, VCSEL behavior with respect to structure, temperature and modulation was presented and characterized. To facilitate in the design of an efficient optical system, beam propagation fundamentals were reviewed along with the measurement of optical properties of the available VCSEL array. Progress still has to be made in several areas such as VCSEL packaging and integration to VLSI circuits. On the other hand, the planar construction of the MSM photodetectors make them an ideal candidate for their incorporation into a VLSI electronics processes and a monolithically integrated optical receiver was presented. The next chapter will discuss fiber image guides.

2.6 References

1. R.L. Hartman & al., "Continuous operation of GaAs-$Ga_xAl_{1-x}As$, double heterostructure lasers with 30°C with half lives exceeding 1000h", *Appl. Phys. Lett.*, vol. 24, no. 4, pp.181-183, 1973.

2. K.D. Choquette and H.Q. Hou, " Vertical-Cavity Surface Emitting Lasers: Moving from Research to Manufacturing", *Proc. of the IEEE*, vol. 85, no. 11, pp. 1730-1739, November 1997.

3. J.L. Jewell, J.P. Harbison, A. Scherer, Y.H. Lee, and L.T. Florez, "Vertical-cavity surface-emitting lasers: Design, growth, fabrication, characterization," *IEEE J. Quantum Electron.*, vol.27, pp.1332-1346, 1991.

4. L.A. Coldren, E. Hegblom, E. Strzelecka, J. Ko, Y. Akulova, and B. Thibeault, "Recent advances and important issues in vertical-cavity lasers", *Proc of the SPIE*, vol. 3003, pp. 2-13, 1997.

5. D.L. Huffaker, L.A. Graham, H. Deng, D.G. Deppe, "Sub-40 μA Continuous-Wave Lasing in an Oxidized Vertical-Cavity Surface-Emitting Laser with Dielectric Mirrors", *IEEE photonics Technology Letters*, vol.8, no. 8, pp.974-976, August 1996.

6. K.L. Lear, K .D. Choquette, R.P. Schneider Jr, S.P. Kilcoyne, and K.M. Geib, "Selectively oxidized vertical cavity surface emitting lasers with 50% power conversion efficiency", *Electronic Letters*, vol. 31, no. 3, pp.208-209, 1995.

7. C.J. Chang-Hasnain, "Semiconductor diode lasers pervade our society", Optics and Photonics News, pp. 35-39, May 1998.

8. K.D. Choquette, K. Lear, R.P. Schneider Jr., K.M. Geib, and H.C. Chui, "Selectively oxidized vertical-cavity lasers," *in Proceedings of the IEEE Lasers and Electro-Optics Society Annual Meeting 1995* (IEEE, New York, 1995), pp.412-413, paper SCl 14.1.

9. B. Weigl, M. Grabherr, C. Jung, R. Jäger, G. Reiner, R. Michalzik, D. Sowada, and K.J. Ebeling, "High-performance oxide-confined GaAs VCSELs," IEEE J. Sel. Top. Quantum Electron. 3, 409-415 (1997).

10. E.M. Strzelecka, D.A. Louderback, B.J. Thibeault, G. B. Thompson, K. Bertilsson, and L.A. Coldren. "Parallel free-space optical interconnect based on arrays of vertical-cavity lasers and detectors with monolithic microlenses", *Appl. Optics*, vol. 37, no. 14, pp. 2811-2821, May 1998.

11. K. Katsura, Y. Ando, M. Usui, A. Ohki, N. Sato, N. Matsuura, N. Tanaka, T. Kagawa, and M. Hikita, "ParaBIT: Parallel Optical Interconnection for Large-Capacity ATM Switching Systems", *IEICE Trans. Commun.*, vol. E82-B, no. 2, Feb. 1999.

12. D.B. Young, J.W. Scott, F.H. Peters, M.G. Peters, M.L. Majewski, B.J. Thibeault, S.W. Corzine, L.A. Coldren, "Enhanced performance of offset-gain high-barrier vertical-cavity surface-emitting lasers," *IEEE J. Quantum Electron.*, vol.29, pp.2013-2022, 1993.

13. P. Schnitzer, U. Fiedler, M. Grabherr, C. Jung, G. Reiner, W. Zich, and L.J. Ebeling, "Bias-free 1 Gbit/s data transmission using single mode GaAs VCSELs at λ=835 nm", Electron. Lett. vol 32, pp. 2145-2146, 1996.

14. Honeywell Optoelectronics Application Sheet, Modulating VCSELs.

15. N.H. Kim, "2-D free-Space Optical Backplane Using Vertical-Cavity Surface-Emitting Laser", McGill University, Master Thesis, 1996.

16. D.B. Schwartz, C.K.Y. Chun, B.M. Foley, D.H. Hartman, M. Lebby, H.C. Shieh, S.M. Kuo, S.G. Shook, B. Webb., "Optobus: A low cost, high performance optical interconnect," *Technical Digest of 45th Electronic Components & Technology Conference (ECTC '95)*, pp. 376-379, May 1995.

17. A.V. Krishnamoorty, K.W. Goosen, L.M. Chirovsky, R.G. Rozier, P. Chandramani, W.S. Hobson, S.P. Hui, J. Lopata, J.A. Walker, and L.A. D'Asaro, "16X16 VCSEL array Flip-chip bonded to CMOS VLSI Circuit", *in Optics in Computing, OSA Technical Digest* (Optical Society of America, Washington, DC, 1999), PD2.

18. J. Tatum, D. Smith, J. Guenter, and R. Johnson, " High Speed Characteristics of VCSELs", Fabrication, Testing, and Reliability of Semiconductor Lasers II, vol. 3004, pp. 151-159, 1997.

19. D.F. Brosseau, "Design, implementation and characterization of a kinematically aligned, cascaded spot array generator for modulator-based free-space optical interconnect", McGill University, Master Thesis, 1999.

20. Y.-G. Zhao and J.G. McInerney, "Transverse-Mode Control of Vertical-Cavity Surfave-Emitting Lasers", *IEEE J. of Quant. Electronics*, vol. 32, no. 11, pp. 1950-1958, Nov. 1996.

21. B.E. A. Saleh, M.C. Teich, Fundamentals of Photonics, John Wiley & Sons, Inc., New York, 1991

22. T.F. Johnson, Jr., "M^2 concept characterises beam quality" *A reprint from Laser Focus World*, May 1990.

23. D. Burak, S.A. Kemme, R.K. Kostuk, and R. Binder, "Spectral identification of transverse lasing modes of multimode index-guided vertical-cavity surface-emitting lasers", *Appl. Phys. Lett.*, vol. 73, no. 24, pp. 3501-3503, 1998.

24. J.M. Senior, Optical Fiber Communications: Principles and Practice, Prentice-Hall International, Inc., London, (1985).

25. J.F. Ahadian, "A Monolithic Very Large Scale Optoelectronic Integrated Circuit Technology" Massachusetts Institute of Technology, Ph.D. Thesis, 1999.

26. D. Wood, Optoelectronic Semiconductor Devices, Prentice Hall, New Jersey, chapter 6, 1994.

Chapter 3

Fiber Image Guides

3.1 Introduction

Flexible coherent fiber bundles also called fiber image guides have been known to provide good image transfer capabilities. Such FIGs have been originally developed to be used as various imaging and sensing tools in medical diagnostics as well as in industrial inspection applications [1-2]. The technology behind FIG's is becoming readily available and relatively mature, making them a low cost alternative for parallel datacom applications. In this chapter, fiber image guides are described in detail with respect to their physical structure and compared to regular fiber optics. Finally, their parallel transmission characteristics are presented and discussed along with design considerations for their use as a two-dimensional medium of data transport.

3.2 Fiber Image Guide (FIG)

Because of their effectiveness in inspection applications, FIG technology is growing rapidly. Various FIGs are now commercially available and several researchers are actively pursuing their use for datacom applications [3-11]. A Fiber Image Guide consists of a coherent bundle of individual step-index fibers. Fiber diameters typically range from 8 to 20 μm and their relative spatial position is maintained throughout the bundle [9]. Higher resolution FIGs can be manufactured and FIGs with a core diameter as low as 0.25 μm have been demonstrated [12]. Typically, up to 20 000 individual fibers can be packaged in a 4 mm^2 image guide, resulting in packing densities up to 0.5 million fibers/cm^2 [8].

FIGs can be made either rigid or flexible. Large FIGs with areas in the order of 25 mm^2 are possible at the expense of bending flexibility. Flexible FIGs are preferred for interconnect applications but individual fiber elements can break internally, whereas with a rigid FIG they will rarely break or break completely. A broken fiber is referred to as a Dark fiber, whereas a fiber which is partially transmitting light is often called a Grey fiber. Therefore per central quality area, FIGs can be manufactured with a total of 0.05% Grey/Dark fibers which is considered acceptable for bundles used in imaging applications [13] and should be sufficient for optical interconnects.

3.2.1 *FIG Manufacturing*

The two most common material for image guides are glass (silica) and Poly(methyl methacrylate) PMMA (polymer) [6]. Glass is usually more expensive but can be manufactured with better optical properties such as higher image resolution (higher pixel count) and smaller fiber cores suggesting larger bandwidths.

The glass image guides obtained from Schott Fiber Optics are flexible in the central section and solid at the edges. To achieve such a structure a specific fabrication process is required. The main steps of the fabrication process are as follows: a core and a cladding material (glass) are used to draw the individual fibers using a traditional method for step index fibers. A third glass around the cladding, or a second cladding must be added if the final product is to be flexible. In this case Acid Soluble Glass (ASG) is used as a second cladding [14]. After the individual fibers are drawn, stacked, and redrawn, a hexagonal array of fibers makes up the bundle. The ASG acts as the cohesive agent between the individual fibers. The ends of this array are waxed and the entire bundle is submerged into an acid bath. All of the ASG in the unwaxed areas dissolves, making the center of the bundle flexible. The ends stay rigid because the ASG is protected by the wax.

3.2.2 *FIG for Parallel Interconnects*

In comparison with fiber arrays, FIGs represent an over sampled approach to parallel optical interconnects, as several fibers are used to transmit each data channel. Noise and

cross-talk problems prevent the use of all the available spatial channels for simultaneous data transmission [3]. Nevertheless, this very high number of fibers significantly relaxes alignment tolerances and ensures that individual fibers can be damaged without loss of a channel. Flexibility is very high and the FIG can easily be bent in a radius of 1 mm.

Several FIGs were obtained from Shott Fiber Optics. The properties of the 1.35m FIG used for most analysis and later in the interconnect system of chapter 4 are summarised in Table 3.1. The cross section of this FIG is hexagonal with a diagonal length of 1.93 mm. The fibers at the ends of the image guide are held in a rigid glass matrix and protected by a metal jacket. The rest of the guide consists of loose fibers in a plastic sleeve. This jacket enables the manipulation of the fiber without damaging it. The image guide is nevertheless fragile, especially near the interface between the rigid and loose fibers and breakage problems may occur at that point. Figure 3.1 shows a cross-section profile of the FIG and its corresponding close-up appearance. The fibers in the bundles are stacked in a hexagonal close-packed structure. Each fiber has six nearest neighbours, all in contact with each other on the perimeter. This makes the center-to-center spacing the same value as the fiber size, or 12.7 microns in this case. For VCSEL based applications the NA (Numerical Aperture) of the FIG should be high enough to match the NA of the VCSEL, therefore a NA of 0.2 would be sufficient.

Parameter	Specification
Cable diameter	1.93 mm
Length	1.35 m
Pixel count	17000
Numerical aperture	0.55
Core index (n_f)	1.58
Cladding index (n_c)	1.49
Fill ratio (%)	~ 55 %
Core size	10.0 μm O.D.
Clad thickness	1.4 μm
Total fiber size	12.7 μm O.D.
Flexibility	Excellent
Manufacturer	Schott Fiber Optics

Table 3.1. Summary of fiber image guide parameters

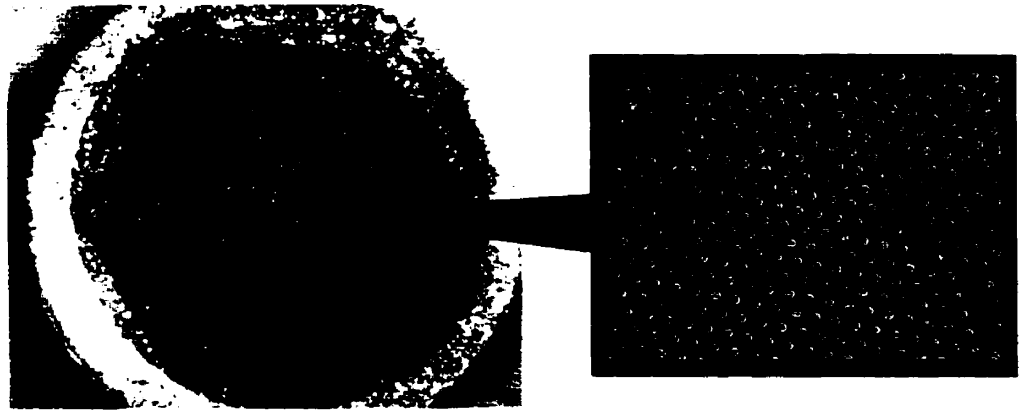

Figure 3.1. Fiber image guide cross-section

3.3 Bandwidth Calculations

Skew and dispersion often limit the maximum bandwidth of a fiber optic communications system. Dispersion causes distortion for both digital and analog signals by resulting in intersymbol interference (ISI). To prevent ISI and have no overlapping of light pulses the digital bit rate (B_T) must be less than the reciprocal of the broadened pulse duration (2τ) [24]. Hence:

$$B_T < \frac{1}{2\tau} \qquad \text{Equation 3.1}$$

Another more accurate estimate of bit rate may be obtained by considering the light pulses at the output to have a Gaussian shape with a rms (root mean square) width of σ. The maximum bit rate is then given by a reasonably good approximation [23]:

$$B_T\,(\max) = \frac{0.25}{\sigma}\ \text{bits / s} \qquad \text{Equation 3.2}$$

Since every channel in a FIG is travelling over several cores, skew or multi-path dispersion can limit per-channel speeds. Further with 10 μm core sizes, these individual

fibers are multimode at 850 nm and modal dispersion will also limit the bandwidth over longer distances. All the optical fibers of a FIG are usually fabricated in the same conditions and their characteristics can be expected to be uniform. Thus skew or time of flight variations due to different fiber lengths and refractive indices should be negligible. Skew itself is difficult to measure but results suggest total pulse broadening, including skew and all dispersions, to be less than 2 ps/m [5]. Several Gbit/s per channel transmissions may therefore be easily achieved for short distances without any significant skew or dispersion [6].

Modal dispersion for a single multimode fiber as used in the FIG can be estimated. Using the ray theory model, the fastest and slowest modes propagating in a step index fiber may be represented by the axial and extreme meridional rays. The time difference between the shortest and longest optical path allows estimation of the pulse broadening resulting from intermodal dispersion. Hence the time difference δT_s may be expressed as follows [24]:

$$\delta T_s = \tau = T_{Max} - T_{Min} = \frac{L n_f^2}{c n_c}\left(\frac{n_f - n_c}{n_f}\right) \qquad \text{Equation 3.3}$$

where L is the length of the fiber, n_f and n_c the core and cladding index of refraction and c the speed of light.

Another useful quantity with regards to intermodal dispersion in an optical fiber is rms pulse broadening. Rms broadening can be expressed in terms of variance σ^2 as follows [24]:

$$\sigma = \frac{L n_f}{2\sqrt{3}\, c}\left(\frac{n_f - n_c}{n_f}\right) \qquad \text{Equation 3.4}$$

Thus the bandwidth for a typical 10 μm fiber core used in the 1.35 m FIG, using equation 3.1, can be calculated to 1.2 Gbit/s. Alternatively using a rms pulse broadening calculation (equation 3.2), the maximum bandwidth yields B_T = 2.1 Gbit/s. These

calculations assume the step index fiber will exhibit large amounts of intermodal dispersion and thus neglects skew and all other dispersions. For such fiber length, cladding modes may exist and over 200 can modes propagate in a 10 μm core at 850 nm.

3.4 FIG Characterization

Before designing any optical interconnect, it is important to understand the transmission characteristics of the transport medium. Several factors which can limit the performance of an optical system based on an image guide have been investigated and measured. Specific characteristics such as coupling uniformity, dispersion, attenuation, bending loss and spot spreading will be discussed in the following sections.

3.4.1 Coupling Uniformity

In a parallel optical transmission system it is highly desirable to receive a predictable and uniform power distribution across the receivers. This simplifies the design of the receiver array by allowing it to have a common threshold (decision) level. It also prevents the need to individually adjust each channel. It is even more important when operating receivers in an optical differential configuration. Non-uniformity of insertion loss is one potential disadvantage of fiber image guides. Although the location of the image guide with respect to a transmitter array and a receiver is known, the energy of a single optical channel is randomly distributed over several cores and cladding. The optical power coupled into the cladding is diffused or combined into adjacent cores.

The power throughput varies depending on the input spot size and position. If a spot is small, almost all of its optical power may be coupled into a single fiber, making it highly efficient, however, if the spot falls on a cladding area, it will perform poorly. As illustrated in Figure 3.2 one logical solution is to increase the spot size. This will allow the spot to couple into several fibers and reduce power variations. However for tightly pitched VCSELs it is desirable to have a smaller spot size in order to prevent crosstalk. There may therefore be a trade-off between spot size and output power uniformity.

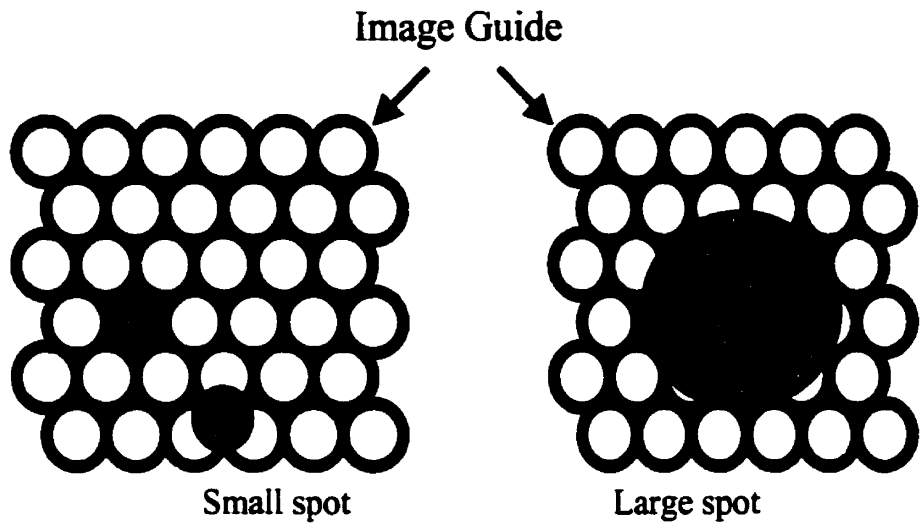

Figure 3.2. Illustration of impact of spot size on coupling uniformity

In order to study power uniformity, the image guide was mounted onto a motorized translation stage and a single VCSEL was set to a continuous wave operation. The experimental setup is shown in Figure 3.3. Two 25mm lenses in a 4f configuration where set to focus the light into the image guide. A power meter recorded the output power as the image guide at the input was translated in two dimensions in steps of 1 μm.

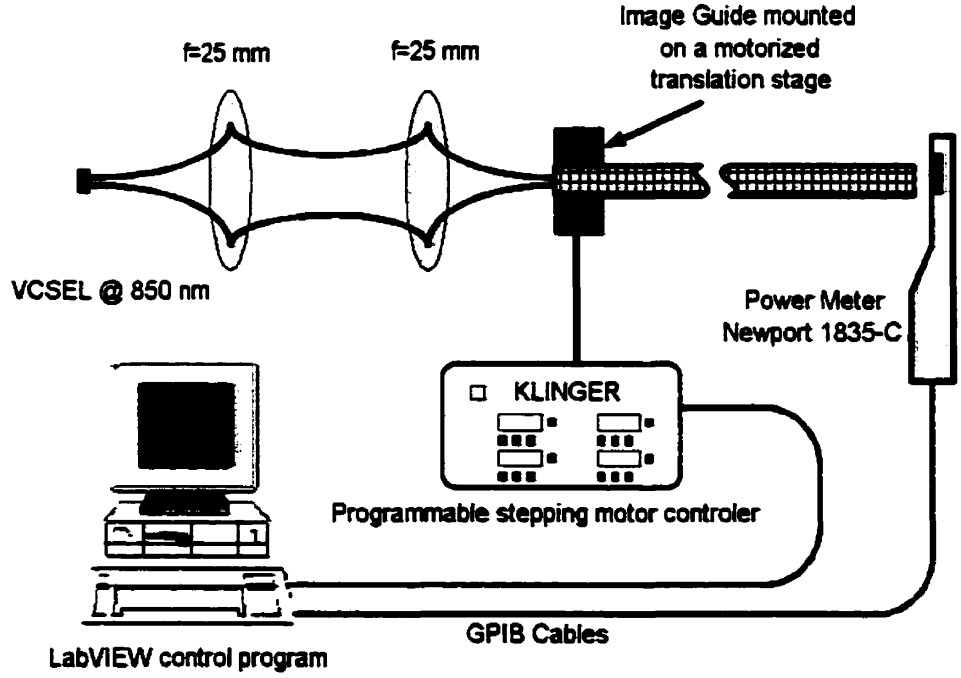

Figure 3.3. Coupling efficiency experimental setup diagram

The experiment was fully automated, a labVIEW software interfaces through GPIB cables to the power meter and to the translation stage. The program controls the stepper motors while acquiring data from the power meter at a 3 seconds interval. All the data is saved in a file which can be used to generate graphs or perform statistical computations.

A typical result is shown in Figure 3.4. Output power variations are clearly visible for a 50 μm spot size. Uniformity across the periodic pattern of cores seems to be constant. By comparing the local maximums it was possible to calculate that the measured throughput does not vary by more than 2% across a 50 X 50 μm FIG area.

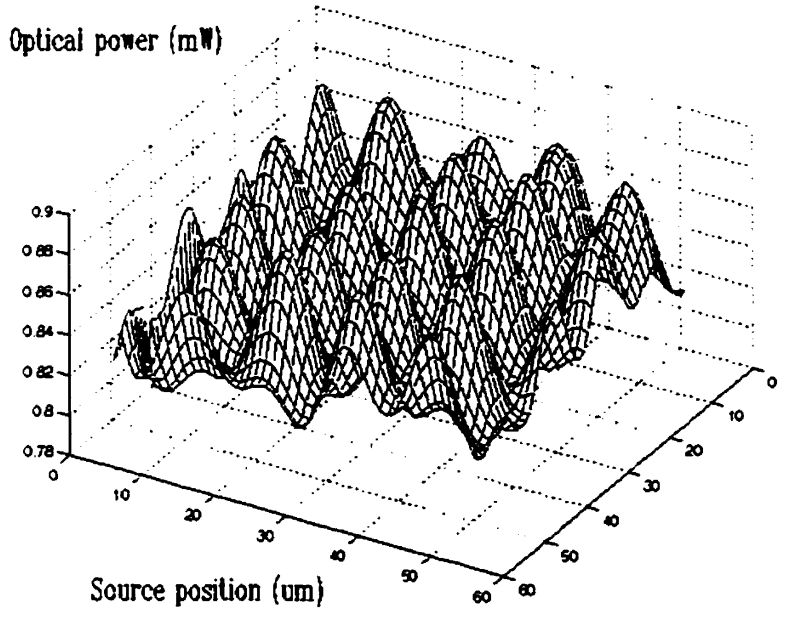

Figure 3.4. Throughput variation with respect to VCSEL-FIG position (spot size is 50μm)

Further to observe the behavior with respect to input spot size a similar analysis was performed with the exception of varying the lens-FIG distance to give different spot sizes. Typical results are shown in Figure 3.5, where for different spot sizes the amplitude of the coupling uniformity clearly varies.

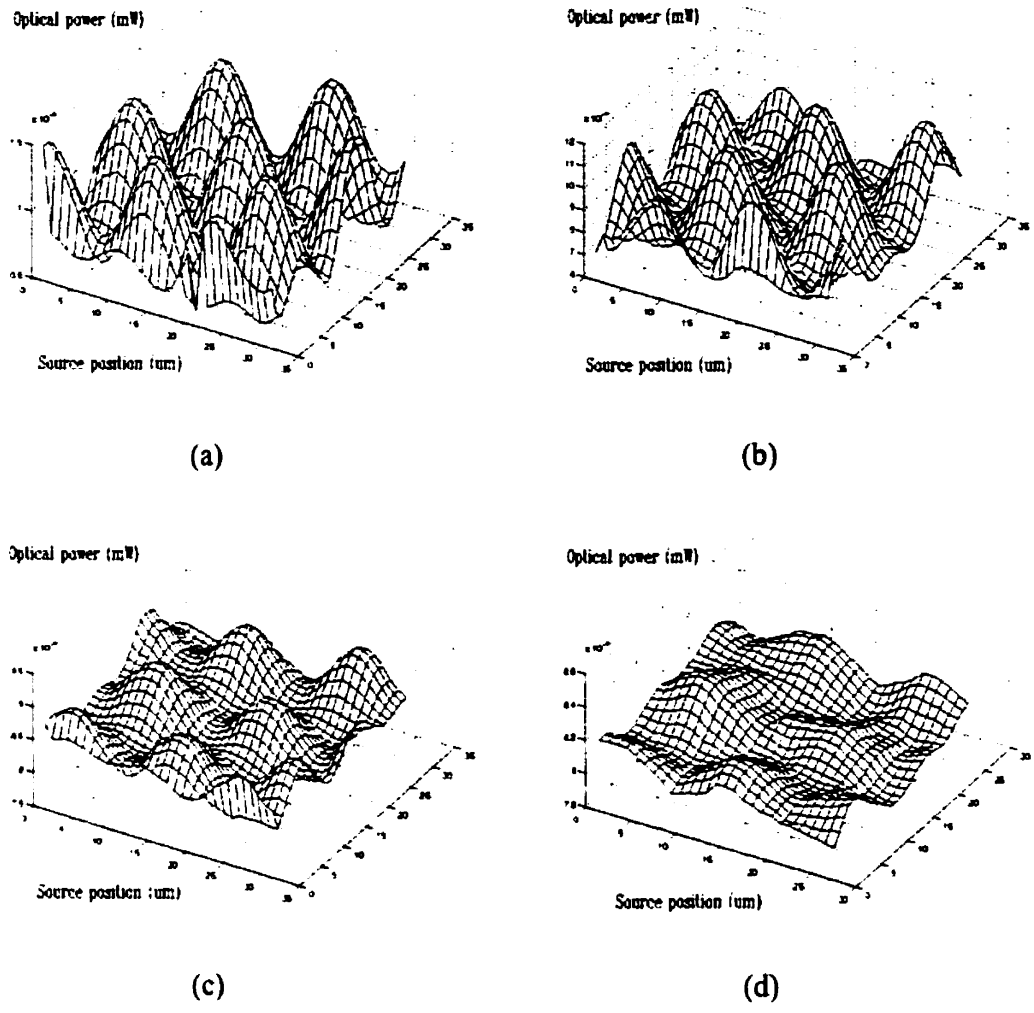

Figure 3.5. Throughput variation with respect to VCSEL-image guide position for different spot sizes, (a) 12 μm, (b) 24 μm, (c) 48 μm and (d) 70 μm

Statistics were computed on the collected data. Figure 3.6 shows the dependence of the maximum, minimum and variance of the output power on spot size. As expected the optical power variation decreases as the spot size is increased. The average power remains almost constant and spot size should be selected depending on the tolerable variations at the receiver as well as crosstalk. Another important issues which should be pointed out, is tilt of the image guide with respect to the image plane. Tilt will certainly reduce coupling efficiency and will certainly change or distort the input spot size.

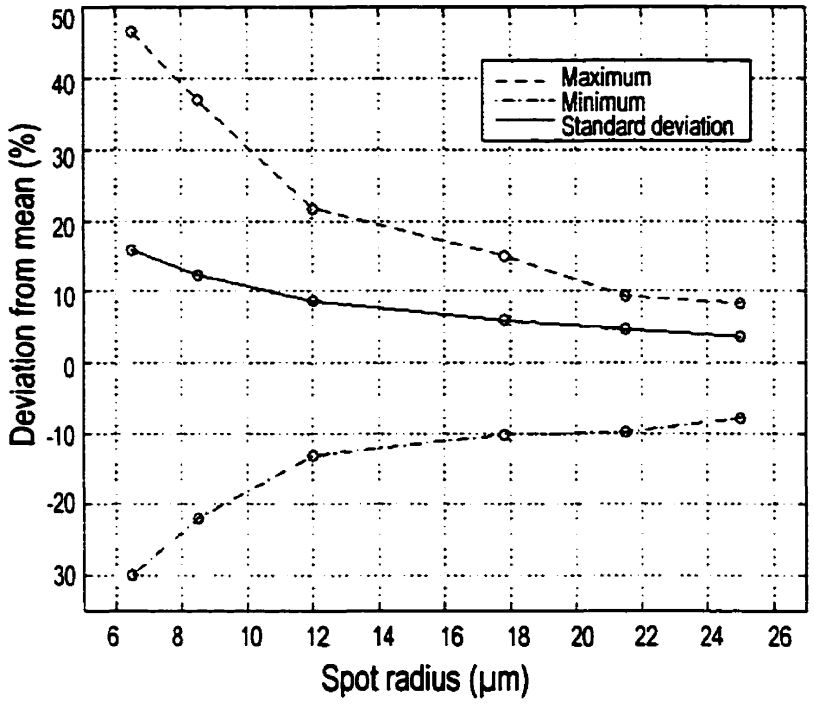

Figure 3.6. Coupling uniformity as a function of spot size at the fiber image guide input face

3.4.2 Attenuation

In long haul fiber optics telecom applications, fibers are designed for minimum attenuation in their respective wavelength windows. Channel attenuation largely determines the maximum transmission distance prior to signal restoration. Attenuation can be in the order of 0.25 dB/km for commercial single mode fibers in the 1550 nm wavelength window [16]. Fiber images guide are not designed for minimum attenuation and their projected use is in the 850 nm window which is far from optimum terms of the attenuation spectrum.

Attenuation less than 0.4 dB/m in the 700-1100nm has been measured [8]. Another reported result suggests a 2.8 dB/m loss at 830 nm [7]. Using a simplified cut-back or differential method [18] (without the use of a mode scrambler and frequency chopper),

several FIGs with different core sizes and NAs have been measured for attenuation. The following relationship for optical attenuation per unit length α_{dB} may be used:

$$\alpha_{dB} = \frac{10}{L1 - L2} \log 10 \left(\frac{P2}{P1} \right) \qquad \text{Equation 3.4}$$

L1 and L2 are the fibers lengths respectively, and P1 and P2 are the corresponding output optical powers at a specific wavelength. Table 3.2 summarises the results as obtained by averaging several trials. The results suggest that a typical glass image guide should not exhibit more attenuation than 2.5 dB/m. This total attenuation includes material attenuation, scattering losses and bending loses. Bending loses will likely be negligible and are discussed in the next paragraph.

Fiber Image Guide Parameters			Results
NA	Core size (um)	Fill Ratio (%)	Attenuation (dB/m)
0.55	20	46	0.86
1	9	46	2.52
0.55	11	76	1.57
1	11	76	2.20
1	20	46	2.48
0.25	9	45	2.36

Table 3.2. Measured FIG attenuation per unit length

Optical fibers suffer radiation losses at bends or curves on their paths. This is due to the energy in the evanescent field at the bend exceeding the velocity of light in the cladding and hence the guidance mechanism is inhibited, which causes the light to be radiated from the fiber [24]. To measure bending loss the FIG was twisted 3 times around a 2mm diameter metal rod but the decrease in output power was not measurable. Further bending of the FIG would risk breakage of individual fibers. At such a high bend radius, it is possible to suspect some radiation losses from individual fibers but simple calculations suggest otherwise. To ensure the light does not escape from a fiber and is re-coupled into an adjacent one without loss of total power, a CCD camera was set-up to observe the FIG

as it was bent. As the FIG was bent, visually, it was impossible to confirm such a theory and as the calculations suggest light does not radiate from individual fibers.

3.4.3 Dispersion

Intermodal dispersion typically limits single multimode fiber to transmission distances of less than 1 km and bit rates of less than 1 Gbit/s. To investigate the high frequency behavior of the image guide, a bit-rate of 1 Gbit/s was transmitted through it. The bit stream was generated from a HP 80000 data generator. A VCSELs was directly modulated and was pre-set to operate at an average power of 2.5 mW which corresponds to a bias current of 8.5mA. The receiver used is an Antel (ARX-SA) high-speed avalanche photodetector with a 3-dB bandwidth of 3Ghz and an adjustable gain. Figure 3.7 (a) illustrates a 1 Gbit/s square wave at the input of the FIG and part (b) shows the same waveform at the output of the FIG (bottom signal is the input electrical signal). These waveform where captured with an 8-points averaging to reduce noise and enable to better compare the waveforms. A ND (Neutral Density) filter was also used when reading the input signal without the FIG.

The transmission through the 1.35 m image fiber appears to shows no visible distortion (dispersion and skew). This result confirms that over such a distance the FIG can easily handle a 1 Gbit/s bandwidth. For an ideal measurement a mode scrambling device should be inserted before the FIG to ensure the excitation of a large number of modes [18]. Further to obtain a suitable dispersion measurement a laser able to generate pulse in the order of 200 fs should be used.

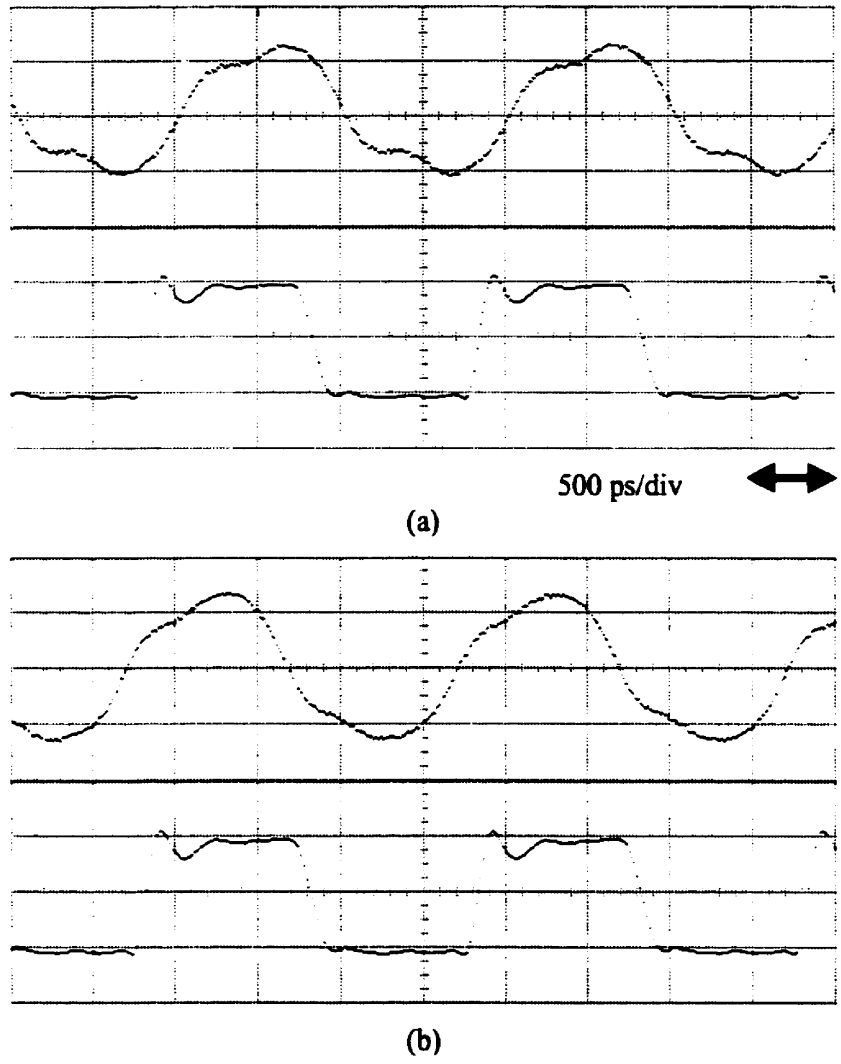

Figure 3.7. (a) 1 Gbit/s square waveform with corresponding input voltage
(b) Waveform at the output of the image guide

3.4.4 Spot Spreading

In single fiber communication, spot size matching is required to increase coupling efficiency between components. Further, extensive analysis of differential mode delay characteristics for today's fiber optic systems has shown that optimum signal propagation distances can be achieved by selectively launching the light into the fiber in a donut shape that encircles the center of the fiber [17]. As demonstrated in chapter 2, at higher bias currents, VCSELs can emit light in a donut shape, however the design objective in a

FIG based system is to couple the light for a channel into several cores, thus making coupling predictions difficult.

When designing optical systems it is often useful to be able to properly model coupling of light into fibers, model propagation of light through waveguides as well as to model beams at their output. Mathematical models for transmitting light through FIGs have not yet been developed. Launching a channel over several cores of a FIG, requires the knowledge of its behavior in terms of spot size to facilitate the design of receiver optics. To minimize crosstalk or to ensure efficient coupling of light on photodetectors, spot spreading is a parameter of interest.

Experiments have reported that a 40 μm diameter spot at the FIGs surface will emerge, after travelling through a 25 cm long FIG, with a beam diameter of 52 um FIG [8]. In order to confirm such numbers spot spreading measurements were performed. Light from a VCSEL was collimated and focused. A Hitachi linear CCD camera with a ND filter of 3.0 is first used to record the minimum input spot size. To couple this spot into the FIG, the image guide is then placed in that plane and the spot is centered on a fiber. As shown in Figure 3.8 the same CCD camera then records the output spot size by focusing on the output plane of the image guide. It is quite difficult to accurately measure the spot size since the camera becomes easily saturated and the ND filter creates some undesirable fringes that distort the image. None the less spot size estimates were obtained by looking at illuminated neighboring fibers and a typical profile is shown in Figure 3.9.

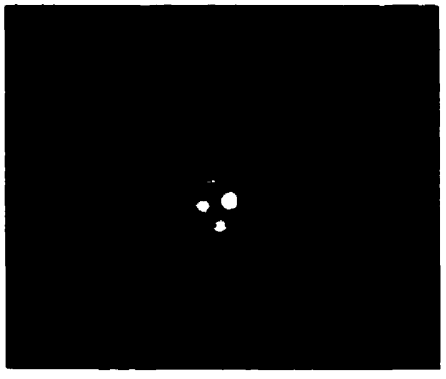

Figure 3.8. Typical spot as recorded with a CCD camera

Qualitatively, results suggest that the output spot size is slightly larger at the output implying limited spot spreading; likely to one adjacent fiber. This might be a direct result of the light being launched into the cladding and re-coupled into an adjacent fiber. Otherwise spot spreading will result from leakage due to bending loses, scattering loses or fiber irregularities.

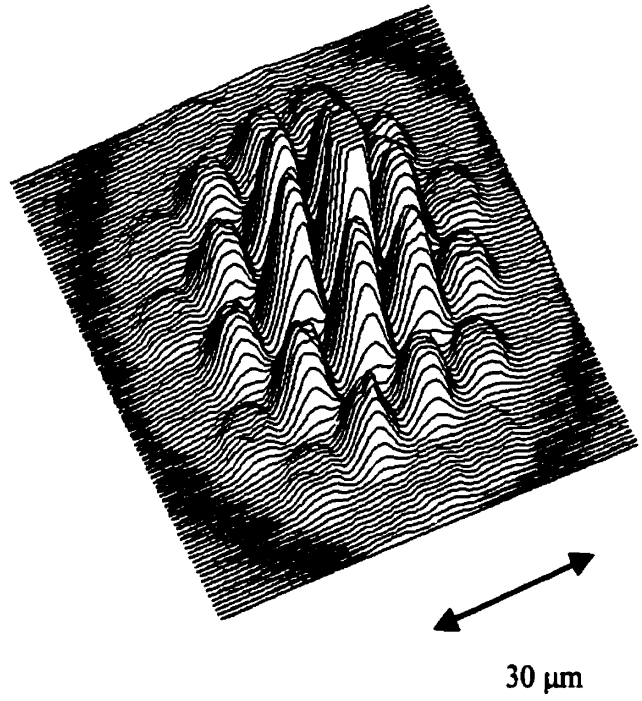

Figure 3.9. Spot profile as measured with a CCD camera

3.5 Optical Feedback

In edge-emitting semiconductor lasers external back reflections will strongly affect their threshold and spectral characteristics [19]. VCSELs, despite their significantly different structures from conventional edge-emitting lasers will experience a comparable behavior to optical feedback. Broadening of the transverse mode spectrum and the appearance of compound-cavity modes have been observed [20]. It has been demonstrated that very low feedback levels (-80dB ~ -20 dB) will alter spectral characteristics of a VCSEL [21].

External optical feedback in a VCSEL based optical system is therefore not a desirable attribute. Modal output power will vary as a result of transverse modes being excited or suppressed depending on the feedback phase. As a consequence, fiber butt coupling efficiency into multimode fibers will be crucial depending on the laser-fiber distance. In practical system, small laser-fiber variations due to thermal expansion or vibrations might cause coupled power to vary by 8-dB for index guided VCSELs [22]. However, for weakly guided proton-implanted VCSELs such as the ones available in the 8X8 array, coupling efficiency will remain well below 0.5-dB [22].

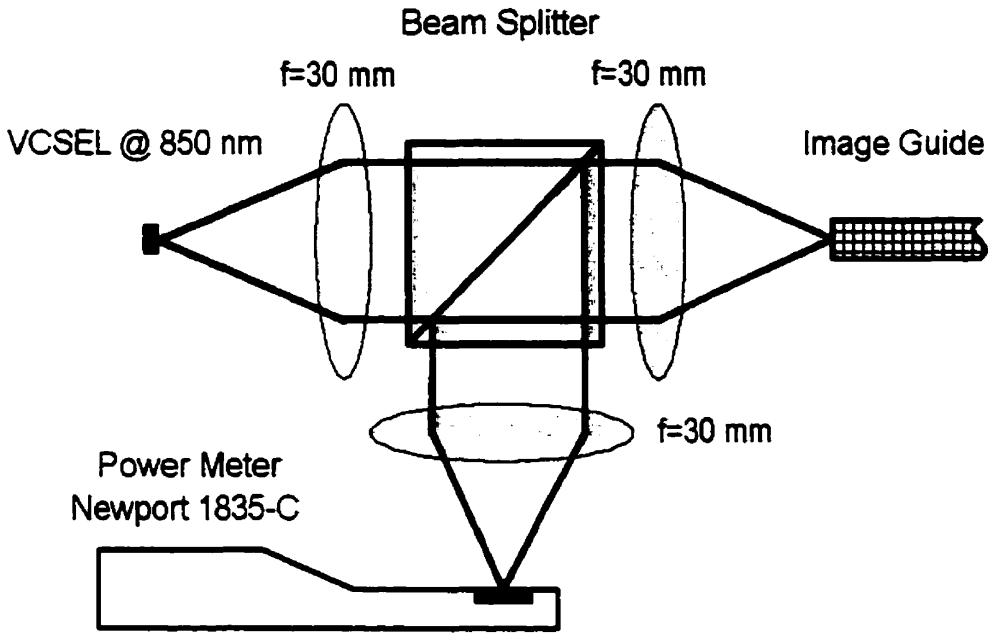

Figure 3.10. Experimental set-up for FIG back reflection measurements

An experimental system was set-up to investigate the reflections at the surface of the FIG resulting from inefficient coupling. The diagram in Figure 3.10 illustrates the experimental set-up used to quantify feedback. A CW (continuous wave) VCSEL operating at 840 nm was maintained within 0.1°C at room temperature. To account for reflections and loss in the optical set-up, a $\lambda/10$ mirror is first used instead of the FIG. The laser beam is reflected back using a flat mirror and a beam splitter is used to couple out the reflected beam. A power meter then measures the reflected power. Once this

measurement is completed the mirror is replaced with a FIG and the power is again measured.

The distance of the FIG was varied to account for different spot sizes and thus different coupling efficiencies. The experiment yielded on average a directional back reflection from the surface of the FIG of less than 6%. This result was obtained, assuming the mirror is 100% reflective, by simply dividing the power measured from the FIG by the power measured from the mirror. In a butt-coupling approach back-reflection might therefore cause a problem and Anti-Reflection (AR) coating the FIG should be considered.

3.6 Conclusion

As demonstrated in this chapter, image guides provide acceptable transmission characteristics and physical properties to be considered for commercial two-dimensional optical interconnects. The bandwidth for short image guides was sufficiently high and signal degradation at 1 Gbit/s from a VCSEL source was negligible. The total attenuation and coupling loss can be expected to be less than 10-dB for a meter long FIG. At present, small spots suffer a high non-uniformity in coupling efficiency due to the probability of the centre of a spot missing a fiber core. Since an uniform and repeatable coupling efficiency is highly desirable, this also suggests that the fiber pitch should be as small as possible to have a high fill ratio. As the trend in transmitter and receiver array pitch decreases towards 62.5 μm, fiber cores might have to decrease in order to allow uniform coupling efficiencies while permitting transmissions of signals over longer distances at rates up to 2.5 Gbit/s. FIGs provide good imaging capabilities with a high resolution while having limited spot broadening for multi-channel transmissions. Finally, back reflections, might represent a problem in future systems based on image guides butt-coupled to oxide-confined VCSEL. The next chapter presents aspects of the design and implementation for the image guide based system.

3.7 References

1. Y. Chugs, K. Fujiwara, Y. Hattori, and Y. Matsuda, "Properties of silica glass image fiber and its application," *Optoelectronics*, vol.1, pp. 172-180, 1989.

2. R. Conde, "Image Quality in Microendoscopy: limiting factors." *Proc. SPIE*, vol. 2048, pp. 243-250, 1993.

3. Y. Li, T. Wang, H. Kosaka, S. Kawai, and K. Kasahara, "Fiber-image-guide-based bit-parallel optical interconnects," Appl. Opt., vol 35, 6920-6933, 1996.

4. H. Kasada, M. Kajita, Y. Li and Y. Sugimoto, "A two-dimensional optical parallel transmission using a vertical-cavity surface-emitting laser array module and an image fiber." IEEE Photon. Tech. Lett. 9, pp. 253-255, 1997.

5. S. Kawai, Y. Li., and T. Wang, "Skew-free optical interconnections using VCSEL-based fiber image-guides," in *The Sixth Microoptics Conference and the Fourteenth Topical Meeting on Gradient Index Optical Systems*, MOC/GRIN Technical Digest (The Japan Society of Applied Physics, Tokyo, 1997), pp. 78-80, 1997.

6. Y. Li, T. Wang, and S. Kawai, "Distributed crossbar interconnects with vertical-cavity surface-emitting laser-angle multiplexing and fiber image guides", Appl. Opt. 37, pp. 254-263, 1998.

7. J. Ai and Y. Li, " Polymer fiber-image-guide-based embedded optical circuit board", *Applied Optics*, vol. 38, no. 2, pp. 325-332, January 1999.

8. K. Tatah, D. Filkins, B. Greiner, and M. Robinson, "Performance measurements of fiber imaging guides and fiber bundles on optical interconnect applications", in *Optics in Computing*, OSA Technical Digest (Optical society of America, Washington DC, 1999), pp. 115-117, 1999.

9. D.M. Chiarulli, S.P. Levitan, P. Derr, R. Menon, and N. Wattanapongsakorn, "Multichannel optical interconnections using imaging fiber bundles", in *Optics in Computing*, OSA Technical Digest (Optical society of America, Washington DC, 1999), pp. 112-114, 1999.

10. T. Maj, A. Kirk, D. Plant, J. Ahadian, C. Fonstad, K. Lear, K. Tatah, M. Robinson, J.A. Trezza, 'Interconnection of a 2D VCSEL array to a receiver array via a fiber image guide', PDP3, *Optics in Computing*, OSA Technical Digest (Optical society of America, Washington DC, 1999).

11. K. Kitayama, M. Nakamura, Y. Igasaki, and K. Kaneda, "Image Fiber-Optic Two-Dimensional Parallel Links Based Upon Optical Space-CDMA: Experiment", *J. of Ligthwave Tech.*,vol. 15, no. 2, pp. 202-212, Feb. 1997.

12. H.F. Ghaemi, Y. Li, T. Thio, and T. Wang, "Fiber Image Guide with subwavelength resolution", *Appl. Phys. Lett.*, vol. 72, no 10, pp. 1137-1139, March 1998.

13. K. Tatah, Schott Fiber Optics Inc., private communication.

14. C.V. Cyan, "Two-dimensional multimode fibre array for optical interconnects," *Elec. Lett.*, vol. 34, pp. 586-587, 1998.

15. J.M. Senior, Optical Fiber Communications: Principles and Practice, Prentice-Hall International, Inc., London, (1985).

16. Corning Inc., Infinicor CL 1000 fiber, Product information sheet.

17. J.W. Scott, "Vertical-Cavity Lasers Facilitate Gigabit Communications", *Laser Focus World*, vol. 34, no 10, pp. 75-79, October 1998.

18. D. Derickson, Fiber Optic Test and Measurment, Prentice-Hall, Inc. New Jersey, 1998.

19. J.H. Osmundsen and N. Gade, "Influence of optical feedback on laser frequency spectrum and threshold conditions", *IEEE J. Quantum Electron.*, vol. QE-19, pp. 465-469, 1983.

20. S. Jiang, Z. Pan, M. Dagenais, R.A. Morgan, and K. Kojima, "Influence of External Optical Feedback on Threshold and Spectral Characteristics of Vertical-Cavity Surface-Emitting Lasers", *IEEE Photo. Tech. Lett.*, vol. 6, no 1, pp.34-36, January 1994.

21. Y.C. Chung and T.H. Lee, "Spectral characteristics of Vertical-cavity surface-emitting lasers with external optical feedback", *IEEE Photon. Technol. Lett.*, vol. 3, pp. 597-599, 1991.

22. J. Heinrich, E. Zeeb, and K.J. Ebeling, "Transverse Modes under External Feedback and Fiber Coupling Efficiencies of VCSEL's", *IEEE Photo. Tech. Lett.*, vol. 10, no 10, pp.1365-1367, October 1998.

23. I.P. Kaminow, D. Marcuse and H.M. Presby, "Multimode fiber bandwidth: theory and practice", *Proc. of the IEEE*, Vol. 68, no 10, pp. 1209-1213, 1980.

Chapter 4

Design and Implementation of FIG based Optical Interconnect

4.1 Introduction

A bit-parallel optical interconnect demonstrator based on a flexible two-dimensional fiber bundle was built. This system demonstrates the feasibility of a high-density optical interconnection for relatively short distances: typically from half a meter to a few hundred meters. At present, commercial optical fiber data links are dominated by fiber ribbons and the total of parallel channels does not exceed a dozen [1-3]. However, due to their linear nature, fiber ribbons do not scale well and two-dimensional formats may be required as the width of computer buses will likely continue to increase [4]. This demand for high-density parallel interconnections might justify the use of an image guide. In this chapter, the design and implementation of a 10 channel parallel optical interconnect consisting of a two-dimensional array of vertical-cavity surface-emitting lasers, a 1.35 m fiber image guide, and a metal-semiconductor-metal receiver arrays is described. All major aspects of the system such as electronics, packaging, optics and optomechanics will be presented.

4.2 System Overview

The implementation of the unidirectional optical data transmission system is depicted in Figure 4.1. The light emitted from the VCSEL array is imaged onto the entrance face of the image guide with the use of 1:1 imaging optics. The lenses in this optical system are mounted in a custom designed barrel which is secured within an optomechanical structure on the printed circuit board (PCB). The light emitted from the far end of the image guide is imaged onto the detector array with a similar optical system. The image guide mount at the receiver permits the FIG to be translated and rotated in order to align all the channels

to the detector array. The link is not designed to support any processing capabilities and a digital data transfer takes place asynchronously with each channel operating independently of others.

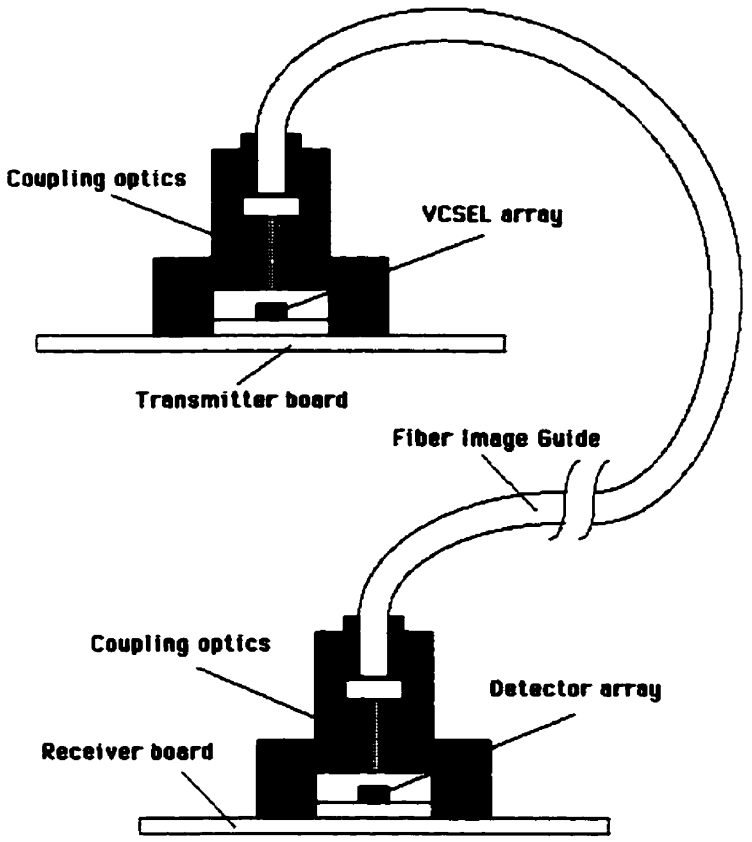

Figure 4.1. Fiber image guide interconnection system

4.3 Transmitter and Receiver Modules

Custom PCBs are used to support electrical off-the-shelve components and active optoelectronic devices. In the next two sub-sections, electrical and packaging aspects of this system will be summarised.

4.3.1 Transmitter and Receiver Layouts

The VCSEL drivers and electrical packaging employed here have been described previously [5]. The requirements for driving a VCSEL are to provide a constant current

source in order to bias the VCSEL and a current swing to modulate the device. Since the system operates with voltage sources, a bias-tee and a current source (LM334Z) are used to convert the voltage into a bias current. The modulation is however an AC voltage modulation. Figure 4.2 shows a diagram of the driver circuit for a single channel. The bias-tees are PCB mountable and are packaged into metal cans. Three boards make up the transmission system, they are connected through an impedance matched (50 Ohms) microstrip ribbon cable from AMP (3GHz 3dB bandwidth).

These boards were designed and fabricated to operate 16 channels simultaneously. The available 8X8 VCSEL array contains 4 times more channels. It is therefore impossible to operate all 64 channels independently. An alternative was to do 4:1 fan-out. However, the available current sources (LM334Z) cannot sink more current than 10mA making a fan-out impossible. The VCSEL chip was wire-bonded with only 16 lasing pixels. From the array symmetry the individual channels were distributed such as to cover as many possible locations (from center to outer corner) while remaining conveniently distributed for later measurements.

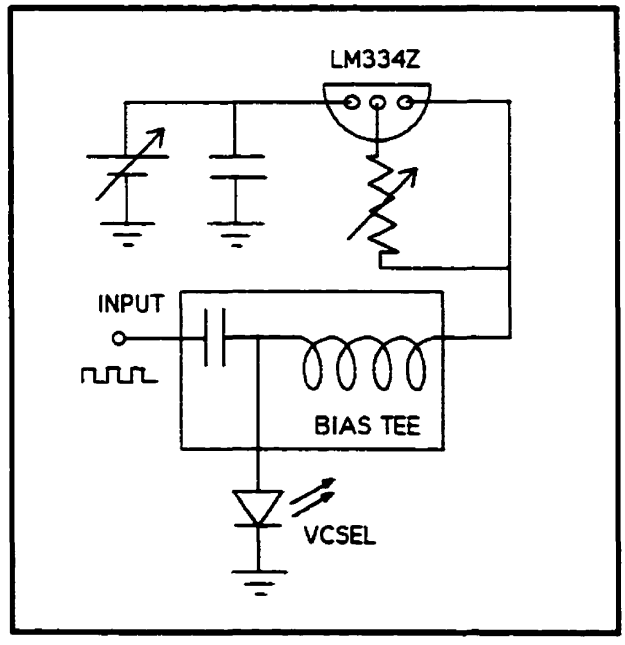

Figure 4.2. VCSEL driver circuit schematic

As described in chapter 2, the receiver die is a monolithic GaAs integrated circuit with MSM detectors and ECL output drivers. Therefore the receiver does not require any other external circuits, it only requires to be properly package on a PCB board with appropriate transmission line characteristics for a high-speed parallel data link.

4.3.2 Packaging and Cooling

The VCSEL die was packaged into a 68-pin CPGA (Ceramic Pin-Grid-Array) chip carrier. Under a microscope the die was centered in the CPGA with tweezers and glued to the CPGA cavity. A chip thermistor was also inserted into the cavity. The array and thermistor were wedge-bonded to the package with 0.7 mil (17.78 μm) gold wire using a K&S wire-bonder. Wire-bonds have been estimated to contribute an inductance of 1nH/mm [6]. Therefore they were kept as short and as flat as possible to preserve bandwidth and also to accommodate for the short working distances of the optics (described in section 4.5).

Similarly to the VCSEL array, the receiver die was centered, glued and directly wire-bonded onto a generic test PCB [7]. The test board includes four copper layers and was designed to support a variety of applications. To minimize crosstalk the generic board was directly connected to a SMA break-out board i.e. without the use of a ribbon cable. The test PCB permits high-speed access to the output of all 16 channels and all the traces have been designed to have a 50 Ω impedance.

A TE cooler and a heat sink where glued in the back of the CPGA for temperature control. The TE cooler is specified to handle of up to 2.6 Watts and the VCSEL array is not expected to dissipate on average more than 100 mW. A LJX temperature controller was used to control the temperature. During experiments a fan was externally mounted to favor heat dissipation. Thermal control was disregarded at the receiver due to the low heat dissipation of the receiver.

4.4 Fiber Image Guide

The available 1.35m Fiber Image Guide used as the optical transport medium for the optical interconnect system was discussed in detail in chapter 3. The cross section of the image guide is hexagonal with a diagonal length of 1.93 mm which does not cover the entire area of the 8X8 VCSEL array. Its area is however sufficient to cover the entire 4X4 receiver die. For these reasons, most of the characterization in the next chapter was performed on the central 10 wire-bonded VCSELs. The fibers at the ends of the image guide are held in a rigid glass matrix and protected by a metal jacket. Optomechanical elements discussed in section 5.5.1 attach with set-screws to the to metal jacket and enable the FIG to be connectorized to the optical link.

4.5 Optical Considerations

Imaging optics were required to couple the light emitted from the VCSELs onto the image guide, and from the image guide to the receiver array. This approach was chosen over butt-coupling [3] the VCSEL directly to the fiber image guide due to the presence of wire bonds at the VCSEL and receiver chip. Complex packaging which permits alignment of the image guide to the detector array would also have been required. Further, the high NA of the FIG would make it difficult to maintain spot size below 70 μm at the detector plane. A bulk lens design was selected in favor of a microlens array (i.e. one microlens for each VCSEL) for reasons of packaging simplicity and ease of alignment of the optical system. Finally, a simple bulk lens system was convenient since the main intention of this demonstrator was to evaluate the performance of the FIG.

Figure 4.3 shows a schematic diagram of the optical system. To properly design the coupling optics, the lens must be carefully chosen to have the smallest amounts of aberrations when coupling the light onto the FIG and then onto the detectors. The optical system was constrained by the high divergence of the VCSELs which required an imaging system with a high numerical aperture (NA) and a relatively large field of view. The field of view necessary to image the entire 1.75 X 1.75 mm VCSEL array limited the

number of suitable commercially available lenses. Further, lenses associated with a large field of view are usually complex, expensive and multi-element. Since the detectors and VCSEL are on the same pitch (250 μm) it was favorable to use a simple 1:1 optical imaging system instead of a demagnification / magnification approach [9]. Therefore the optics for the transmitter and the receiver were based on a 4f or telecentric configuration with two four element, objective lenses. Details of the optical design will be discussed in the following sections.

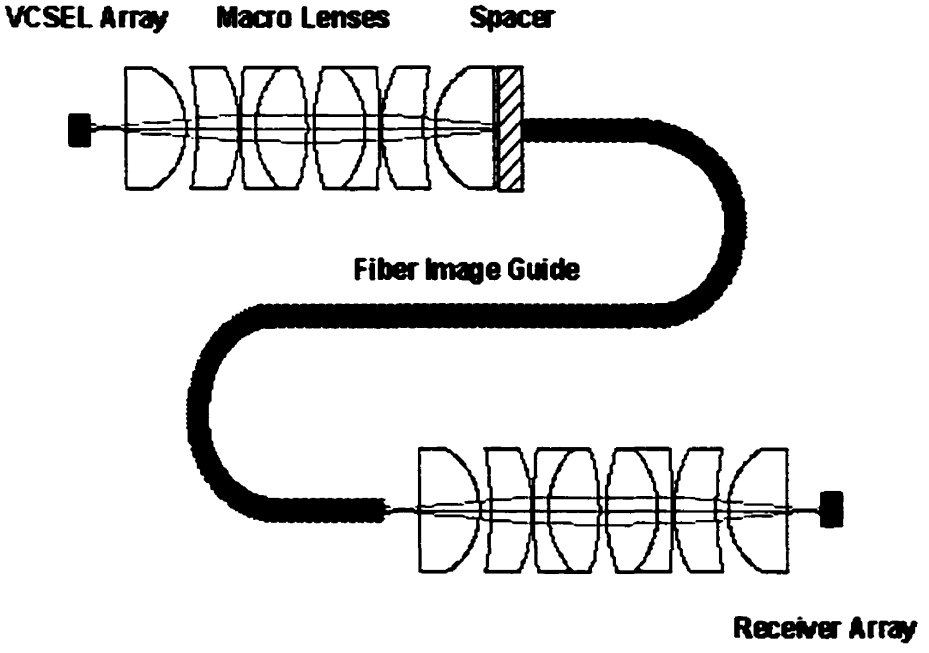

Figure 4.3. Optical system schematic

4.5.1 Aperture

For a simple lens the flux density at the image plane varies as $(D/f)^2$ and the ratio D/f is known as the relative aperture [10]. The focal ratio or f-number (f/#) is an indication of the light gathering power of a lens:

$$f/\# = \frac{f}{D} \qquad \text{Equation 4.1}$$

The divergence of the VCSELs (typically 20° FWHM) requires fast lenses with a working f/# of less than 2.

The amount of energy gathered by a lens from a distant source will be directly proportional to the area of the lens, or more generally, to the area of the entrance pupil. In order to collect the maximum optical energy from the outer most VCSEL, it is important to select a lens with a sufficiently large clear aperture or clear diameter. Assuming a gaussian distribution, a diameter on the lens of 3ω, where ω is the beam radius ($1/e^2$), will collect 99% of the incoming optical power. Figure 4.4 illustrates the requirements for the 8X8 VCSEL array on a 250 μm pitch and which has an outer most VCSEL 1.237 mm from the center of the array.

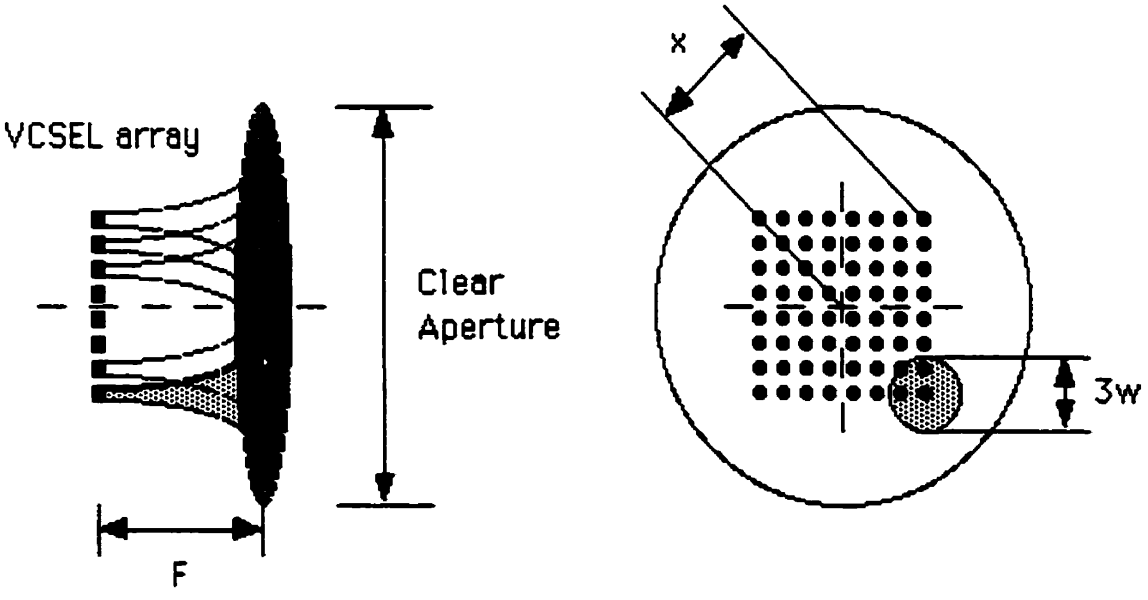

Figure 4.4. Aperture requirements for bulk lenses

To calculate the minimum aperture size D equation 4.2 was used [11]. Where x is the distance between the corner VCSEL and the center of the array, f is the focal length and ω_o is the beam waist ($1/e^2$ radius) of the VCSEL.

$$D > 2x + 3\omega = 2x + 3\omega_0 \sqrt{1 + \left[\frac{\lambda f}{\pi \omega_o^2}\right]^2} \qquad \text{Equation 4.2}$$

Since compound lenses were selected and the modal profile of the VCSEL is not entirely gaussian equation 4.2 was modified to correspond to a ray trace model:

$$D > 2x + 3 f_b \tan\theta \qquad \text{Equation 4.3}$$

where f_b is the back focal length (distance from the VCSEL plane to the vertex of the first lens) and θ is the half angle of the array. For the 8X8 VCSEL array, x = 1.237 mm, the measured half angle is ~10°, and the back focal length of the selected compound lens, f_b, is 1.22mm. Therefore the clear aperture has to be practically larger than 3.12 mm. The oversized Melles Griot lenses with a clear aperture of 8.0 mm exceeded this criteria.

4.5.2 Geometrical Aberrations

Before selecting the lenses, geometric aberrations of the optical system were evaluated for several off-the-shelf lenses by a commercial ray tracing software package, OSLO six. The key design criterion was to keep spot size smaller than 70 μm in order to accommodate for the 75 μm diameter detector area. Aberrations are critical to overall system performance. The outer most VCSEL is the most sensitive to spherical aberrations.

The selected Melles Griot lenses are each composed of four elements and are optimized for a wavelength of 830nm. They are diffraction limited and corrected for spherical aberration, coma and astigmatism. They are also anti-reflection coated for 830 nm with MgF_2. Figure 4.5 shows the lenses in the housing and their properties are summarised in Table 4.1.

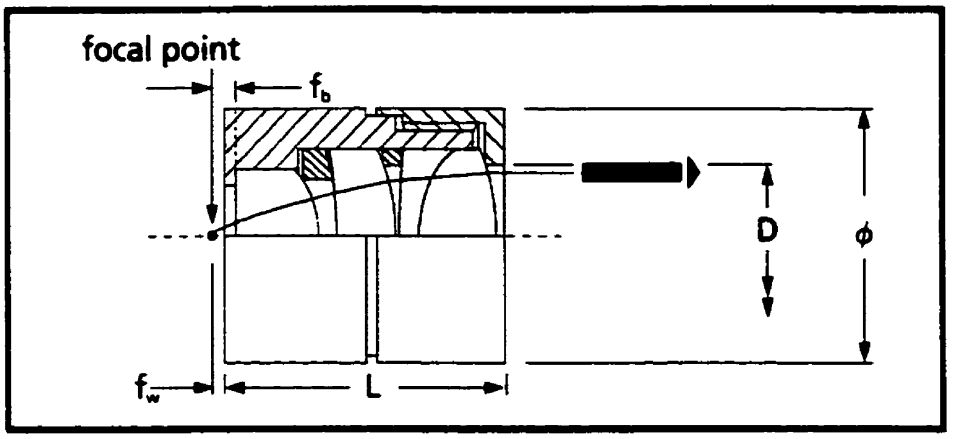

Figure 4.5. Melles Griot collimating and focusing lens

A ray-trace simulation analyzed four VCSELs; they correspond to the VCSELs on the diagonal from the center of the chip. In order to optimize the average spot size for transmission, the on-axis focal plane was defocused i.e. moved forward by 0.1 mm. This focus shift resulted in a smaller spot size for outer VCSELs at the expense of the diffraction limited spot size of the center VCSELs. As discussed in chapter 3, it is in fact beneficial not to have diffraction limited spot sizes at the input of the image guide. However, note that defocusing the spots would not be a viable solution for a bi-directional system because of the symmetry requirements.

Selected Lens	Description/Specifications
Model	Melles Griot 06 GLC 001
Focal length (f_o)	6.5 mm
Numerical Aperture (N.A.)	0.615
Clear Aperture (D)	8.0 ± 0.5 mm
Working Distance (f_w)	0.78 mm
Back Focal Length (f_b)	1.21 mm
Design wavelength (λ)	830 nm
Length (L)	16.48 mm
Diameter (ϕ)	14.29 ± 0.25 mm
Housing / Finish	Aluminum / Black anodized

Table 4.1. Specifications for the collimating and focusing lenses

Figure 4.6 presents simulation results for spot distribution onto the fiber image guide. Simulation results suggest that none of the 64 VCSELs will have a spot size in excess of 40 μm and for all cases 99% of the optical power will remain confined within a 50 μm spot. From the spot diagram, some spots seem to loose their circular nature and can result in a variable power throughput. But since the VCSELs are individually addressable the power variations can be accounted for. Further, by achieving spot sizes in the order of 40 μm most of the optical power should reach the detectors and optical crosstalk should be limited. It should be noted that for the purpose of the simulations the beam from the VCSELs was assumed to be Gaussian. Therefore the Gaussian apodization option which assigns a Gaussian intensity distribution to the ray-trace was selected.

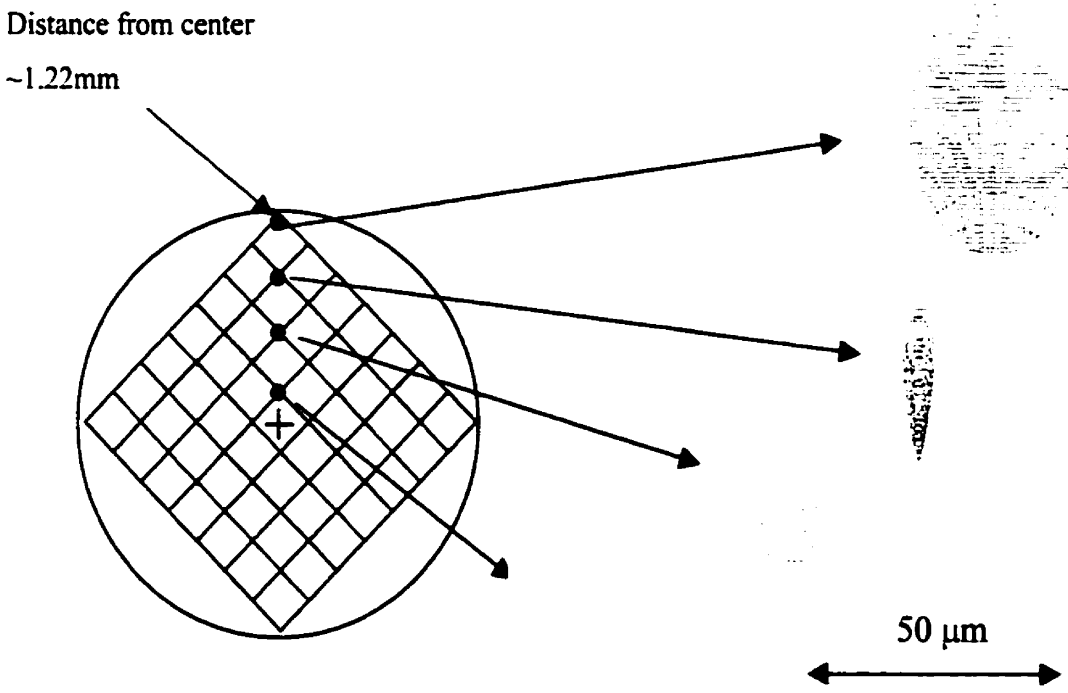

Figure 4.6. Spot pattern at image guide input face

The remaining requirement that was considered in the design of this optical system is distortion. This monochromatic aberration manifests itself in the fact that the transverse magnification may be a function of the off-axis image distance [10]. In the absence of any other aberration, the resulting image might still be distorted even though each point is

sharply focused. Figure 4.7 shows the two types of deformation; barrel and pincushion distortion.

This aberration is particularly relevant to this system since an array is mapped onto another one. Too much distortion will not permit all the optical channels to be efficiently aligned i.e. even if the center channels are perfectly aligned the outer channels may never be. This will degrade the performance of the overall system by increasing crosstalk and decreasing the amount of optical power received at misaligned channels. For the selected lenses, Oslo simulations suggest that the outer most pixel will suffer less than a 0.5% distortion.

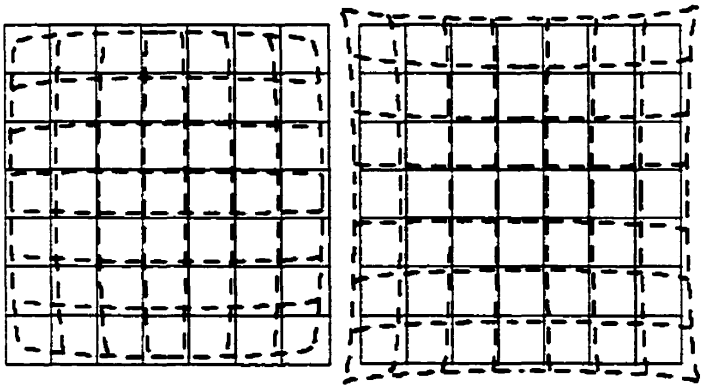

(a) (b)

Figure 4.7. (a) Barrel distortion (b) Pincushion distortion

4.6 Fiber Image Guide Interconnect Implementation

In order to interconnect and align the FIG to the VCSEL array and to the MSM detector array, several aluminum pieces were designed and machined. Details of the transmitter interconnect system are illustrated in Figure 4.8. The optomechanics were designed with high tolerances to establish stable lateral alignment. However, careful longitudinal and rotational alignment will be required during the assembly and alignment of the individual channels. Tilt alignment was not considered in the design of the optical system. With

tight optomechanical tolerances and no system bi-directionality, tilt should be minimal and should not cause any alignment complications.

During the assembly phase, the optomechanics allowed the VCSEL array to be positioned within 50-100 μm of their required location, without any fine alignment, but with careful manipulation of the FIG. Fine alignment was provided by set-screws. The following sections will present the optomechanics and will discuss alignment of the individual optical elements.

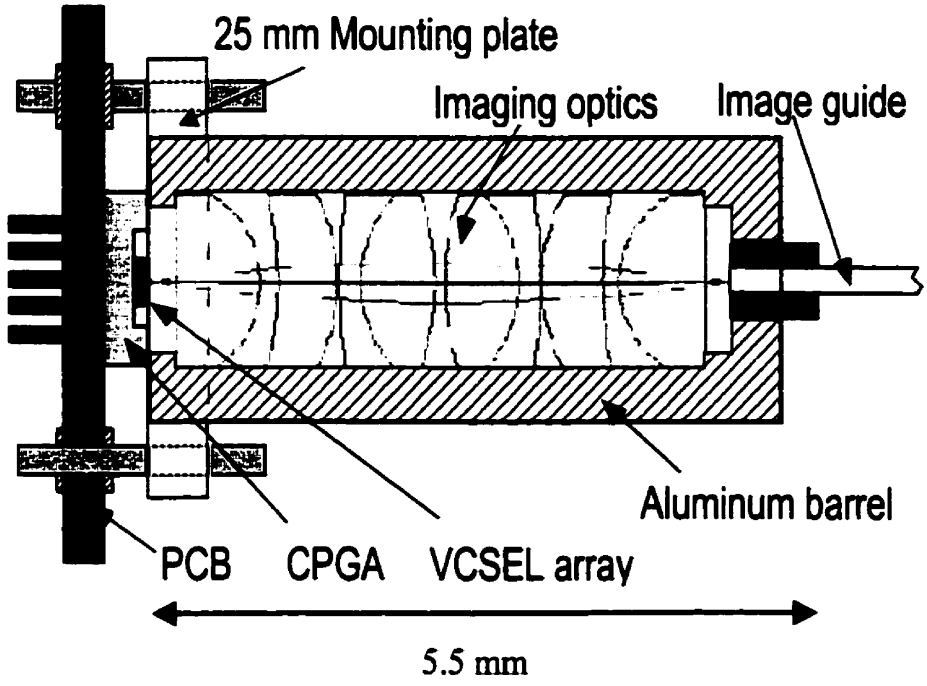

Figure 4.8. Transmission module

4.6.1 Optomechanics

In order to align and interconnect the lenses at the transmission side, the lenses were mounted in a custom designed aluminum barrel. The inner diameter of the barrel was chosen to accommodate the lenses with a tight sliding fit [12]. As shown is Figure 4.8 the barrel is held in a Spindler & Hoyer 25 mm mounting plate and rests with one end on the CPGA. The Fiber image guide is held in a second barrel and is inserted from the other

end. This barrel provides a means for rotational alignment of the FIG. A 0.65 mm custom spacer is used to ensure an optimum distance between the FIG and the second lens. Figure 4.9 shows a picture of the individual elements. The components inside the barrel are locked in place with set-screws. All the set-screws have a nylon tip which prevents any damage on the elements and enables to maintain a tight sliding fit.

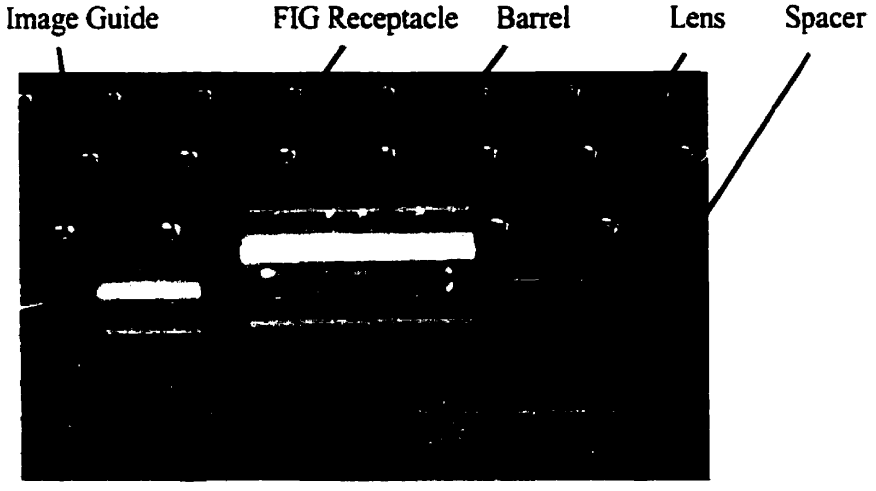

Figure 4.9. Optomechanical components

The barrel holding the two collimating/focusing lenses for the receiver was slightly modified to accommodate alignment of the image guide to the detectors. A stopper was added the barrel and provided stable positioning for the image guide receptacle (barrel). A CAD of the receiver barrel is shown is Figure 4.10.

To make use of the stopper, 45° chamfering was added to the FIGs barrel so that it could be laterally translated with respect to the receiver array with the aid of four set-screws placed 90° apart. As shown in Figure 4.11, the FIG receptacle was intentionally cut (not left circular) so it can be translated in one direction without any set-screws adjustment in the other direction. The total range of movement is 2 mm and the positioning precision is estimated to be between 10 and 20 μm. Finally, as for the transmission side, the barrel is held in a modified Spindler & Hoyer 25 mm mounting plate which itself is attached to the PCB board.

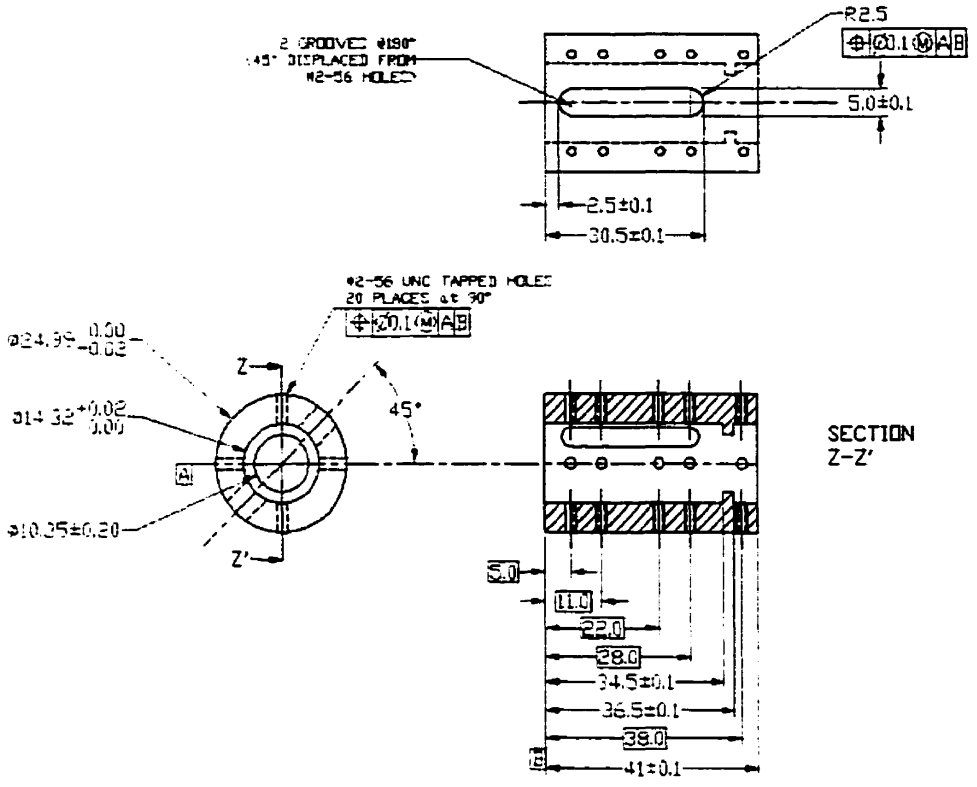

Figure 4.10. CAD drawing of aluminum receiver barrel

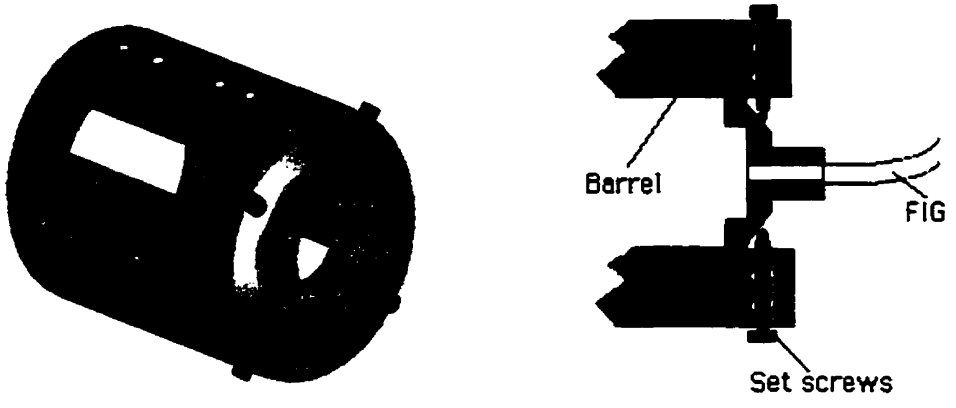

Figure 4.11. Receiver receptacle

4.6.2 Optical System Assembly

The longitudinal alignment of the first lens with respect to the VCSEL array requires active alignment i.e. since the barrel rests on the CPGA the lens must be adjusted until the incoming beam is collimated. A collimation tester has been used to determine the proper distance form the VCSEL. Once this lens is secured inside the barrel the focusing lens can be inserted as well as the 0.65 mm spacer and the FIG. On the receiver side the components should be aligned in a similar fashion; first the FIG should be secured to the barrel and its output should be collimated by actively aligning the first lens. Once this lens is secured the focusing lens can be inserted and the only alignment left over is to the photodetectors.

Two procedures were investigated to align the receiver module to the photodetectors. Since there are no laser sources on the detector plane it is difficult to determine the precise longitudinal location of the die (cannot use a collimation tester), further because of the packaging there is no possibility of inserting a stopper or a spacer. The first approach for lens to detector alignment is to mount the detector module on a X-Y stage and look into the other end of the FIG with a CCD camera. The detector array is translated back and forth with respect to the lenses and barrel until the detector die seen through the camera is in a sharp focus, at this point the alignment should be adequate and the barrel can be secured to the mounting plate.

The drawback to this approach of getting the correct focus is that the alignment is not necessarily optimum for a wavelength of 840 nm but rather for the visible spectrum. Therefore the set-up illustrated in Figure 4.12 can be used. Here the receiver module is again mounted on a translation stage and a CCD camera is used to observe a spot generated from an 840 nm laser source (the FIG aligned to the first lenses must be first removed from the receiver barrel). The receiver module is then translated until the desired spot is achieved on the detector array. At this point, the FIG can the replaced on the stopper and should retain its relative alignment to the first lens while the barrel is locked to the PCB optomechanics.

It should be noted that from ray-tracing simulation spot sizes are quite sensitive to longitudinal displacement. Although these alignment tolerances were not investigated in great detail during the optical design stage, a typical spot in the center of the array can change by up to 10 % by a displacement of 2 μm.

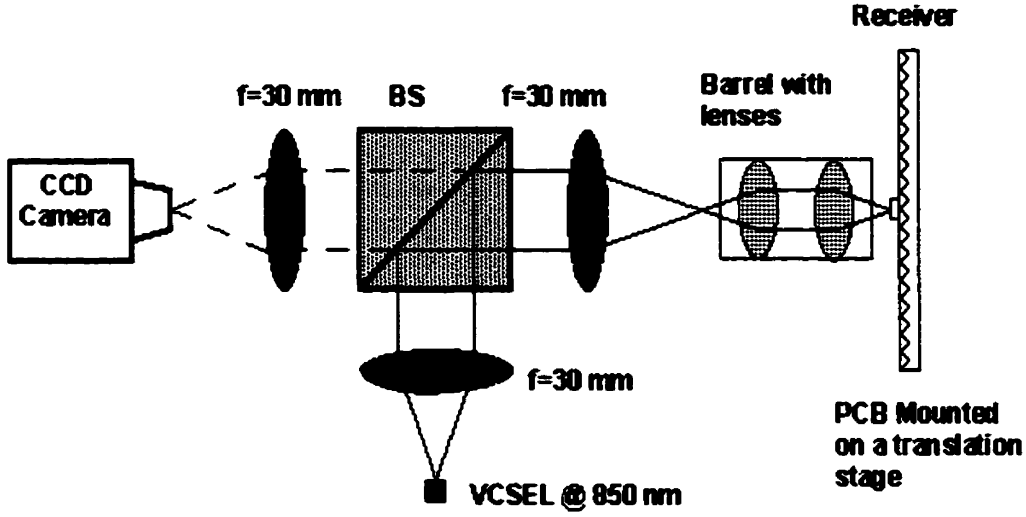

Figure 4.12. Set-up for lens-to-photodetector alignment

4.6.3 Channel Alignment

The selected Melles Griot lenses have a very short back focal length and a relatively small diameter making the entire system compact. Although this is approach is favorable from an esthetic point of view it creates some undesirable complications for alignment. Once the system is assembled there is no way of monitoring the exact location of the spots or channels onto the corresponding detectors i.e. there is not place to insert a beam splitter or a pellicle within the optical system because of the short working distances. Instead, to correctly align the system, the detection of at least two channels must be monitored on a scope and lateral optimization must be made with the use of the set-screws. Rotational alignment can be achieved by rotating the FIG at the transmitter side until optimum performance is seen on the oscilloscope.

4.7 Conclusion

The fiber image guide based link was analyzed from a design perspective. Optical requirements were defined for coupling light into an image guide and onto the photodetectors. A bulk lens coupling approach was selected in favor butt-coupling and microlens based coupling. Optical simulations were performed to select an appropriate lens combination. The selected lenses were four element collimating and focusing lenses optimized for a wavelength of 830 nm. Alignment issues and required optomechanics were also presented along with electrical a packaging concerns for the VCSEL and receiver array. In the next chapter, a complete characterization of the optical link will be presented and discussed.

4.8 References

1. 12L485 VCSEL array and 12L486 PIN array from Mitel Semicondutors, Data sheet.

2. Parallel Optical Links - PAROLI Family, Infineon Technologies (Siemens Corp.), Data sheet

3. Optobus – Motorola: D.B. Schwartz, C.K. Y. Chun, B.M. Foley, D.H. Hartman, M. Lebby, H.C. Shieh, S.M. Kuo, S.G. Shook, B. Webb., "A low cost, high performance optical interconnect," *Technical Digest of 45th Electronic Components & Technology Conference (ECTC '95)*, pp. 376-379, May 1995.

4. Y. Li, T. Wang, H. Kosaka, S. Kawai, and K Kasahara, "Fiber-image-guide-based bit-parallel optical interconnects," *Appl. Opt.*, vol. 35, pp. 6920-6933, 1996.

5. D.V. Plant, B. Robertson, H.S. Hinton, M.H. Ayliffe, G.C. Boisset, W. Hsiao, D. Kabal, N.H. Kim, Y.S. Liu, M.R. Otazo, D. Pavlasek, A.Z. Shang, J. Simons, K. Song, D. A. Thompson, and W. M. Robertson, "4X4 vertical-cavity surface-emitting laser (VCSEL) and metal-semiconductor-metal (MSM) optical backplane demonstrator system," *Appl. Opt.*, vol. 35, pp. 6365-6368, 1996.

6. C.T. Tsai, "Package Inducatance Characterization at High Frequencies", *IEEE Trans. Comp. Pack. and Manufact. Tech.*, vol. 17, no 2, pp.175-181, May 1994.

7. M. Mony, D. Kabal, "Generic Test Board", Internal documentation.

8. Y. Li, T. Wang, H. Kosaka, S. Kawai, and K Kasahara, "Fiber-image-guide-based bit-parallel optical interconnects," *Appl. Opt.* 35, 6920-6933, 1996.

9. Y. Li, T. Wang, and S. Kawai, "Distributed crossbar interconnects with vertical-cavity surface-emitting laser-angle multiplexing and fiber image guides", *Appl. Opt.* 37, pp. 254-263, 1998.

10. E. Hecht, Optics, Addison Wesley Longman, Inc., New York, (1998).

11. Y. Liu "Design, Implementation and Characterization of free-Space Optical Interconnects for Optical Backplanes", Ph.D. Thesis, McGill University, 1997.

12. E. Erik, F.D. Jones, H.L. Horton and H.H. Ryffel, Machinery's Handbook 25, Industrial Press Inc., New York, (1996).

Chapter 5

Performance of FIG based Interconnect

5.1 Introduction

The IEEE has recently completed a Gigabit Ethernet (GbE) standard which enables LANs to transmit data at 1 Gbit/s. To evaluate the potential use of image guides for such applications, the fiber image guide based parallel optical system described in chapter 4 was successfully assembled and characterized. The primary concern was to measure the optical properties of the image guide and the supporting electronics were not specifically designed to operate at gigabit data rates. Only ten channels were transmitted due to in parts to the size of the image guide, to the size the receiver array (4X4) and the channel distribution on the 8X8 VCSEL array. No potential barriers of transmitting all 64 channels through a larger FIG and to a larger receiver array are foreseen.

This chapter begins with a discussion of alignment issues and difficulties encountered during the assembly of the interconnect. Bandwidth performance limitations of the transmitter, the receiver and the entire interconnect will be presented along with a discussion of possible improvements. Finally, system specific characteristics such as optical crosstalk, spot sizes and optical throughput will be presented.

5.2 Alignment

The assembly of the optical and optomechanical components was straightforward. Figure 5.1 shows a picture of the VCSEL array as seen by the receiver i.e. through the FIG and coupling optics. However, simultaneous alignment of all the channels was very difficult since the only way to monitor if a spot was properly aligned with a photodetector was by looking at the ECL output on a digitizing oscilloscope. The interconnection approach

provided a large number of degrees of freedom i.e. lateral alignment, rotational alignments, individual VCSEL bias, and the reference voltage on the receivers. It was often difficult to determine which parameter needed to be adjusted and the alignment was done by trial and error. Once a single channel was aligned for spatial position and transmitted power, it often became poorly interconnected when trying to align the remaining channels. Further, by adjusting the VCSEL bias and receiver reference voltage, a given channel would yield an excellent waveform but it was nearly impossible to determine if it was optimally aligned on a detector i.e. for maximum optical power on the detector. Finally, once two channels of the array became aligned in all three available physical dimensions (x-y and rotation), it became trivial to optimize for transmitted power and all 10 channels would be fully operational in a very short time frame.

Figure 5.1. VCSEL array as seen by the photodetectors

To account for some of these alignment limitations, several improvements are necessary to the image guide and to the connectorization approach. Rotational alignment should easily be solved by manufacturing an image guide with a rectangular metal jacket with corresponding ends for example. Lateral alignment is more difficult to solve but possible

ideas suggest a better connectorization method with guide pins. However the position of the image guide i.e. individual fibers will have to be known with a great precision with respect to the pins. Alternatively the position of the fiber bundle with respect to the outer diameter of the metal jacket must be known with a great precision.

5.3 Bandwidth

When analyzing digital telecommunication systems, single-value waveforms are often not very useful. Real communication systems are not repetitive but rather consist of random bit patterns. A single-value display can only show a few different bit combinations. Pattern-dependent problems such as slow rise time or excessive overshoot will be overlooked if they do not occur in the small segment of pattern appearing on the display.

An eye diagram or eye pattern overcomes these limitations by overlapping all possible one-zero combinations on the oscilloscope. For performance measurements an eye diagram was generated using a Pseudo-Random Bit Sequence (PRBS) and the bandwidth characteristics of the transmitter, of the receiver and of the entire system will be presented and discussed in sections 5.3.1 to 5.3.3.

5.3.1 Transmitter Bandwidth

To characterise the bandwidth of a transmitter channel, an optical test rig was set-up and is illustrated in Figure 5.2. The optomechanics used were Spindler & Hoyer components combined with X-Y stages to facilitate the alignment of the test rig. The light emitted from the VCSEL array was collimated and focused onto the photodetector plane with the use of two f = 25 mm achromat lenses in a 4f configuration. The receiver used was single channel APD photodetector form Antel (ARX-SA) with a 3-dB bandwidth of 3 GHz, a 200 ps rise time and an active area of 0.07 mm^2. The bit stream was generated using an HP 80000 data generator having a 200 ps rise time. The data generator was configured for a NRZ 2^{23} - 1 PRBS with a 0 - 0.4V amplitude swing. The receivers eye diagram was

displayed on a HP 54120 digitizing oscilloscope using a HP 54124A DC to 50GHz sampling unit while triggering of the data generator.

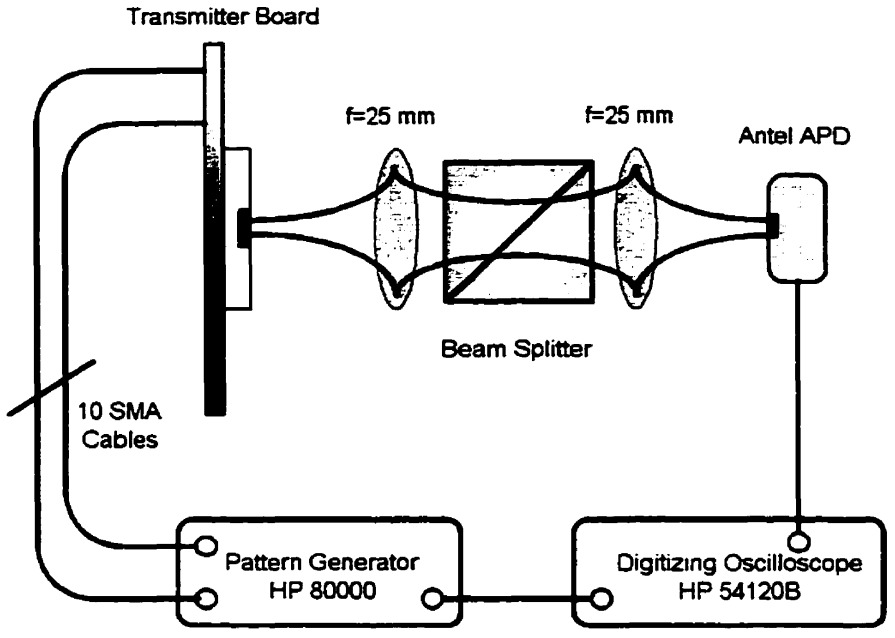

Figure 5.2. Schematic of the test setup

Figure 5.3 shows an eye diagram at 500 Mb/s and 1Gb/s for a single channel under normal operation, i.e. 25°C temperature. The display persistence was set to infinite and the data was collected for approximately 30 seconds. Comparable results were obtained for other channels suggesting a good uniformity across the array. For simultaneous multiple channel operation, the addition of electrical crosstalk within the PCB and especially through the ribbon cables contributed to noise and an overall reduction of bandwidth.

The 3-dB frequency of the VCSELs is higher than 5 GHz and therefore for single channel operation the noise and bandwidth limit can be attributed mostly to the result of cumulative variations in the electrical isolation and layout of the respective electrical components and devices for each channel [10]. To improve performance to gigabit rates it is useful to have proper high-speed laser drivers well packaged on single board which itself is well designed with respect to signal integrity. Selecting higher bandwidth chip

carriers such as ball grid arrays or quad flat packs [1] could achieve further, improved performances. Long wire bonds introduce additional inductance (1nF of per mm for gold wire) [2] but are unavoidable with chip carriers. An optimum approach would be to flip-chip VCSELs to a CMOS chip with laser drivers and then flip-chip the entire package on some type of silicon board to avoid wire-bonds.

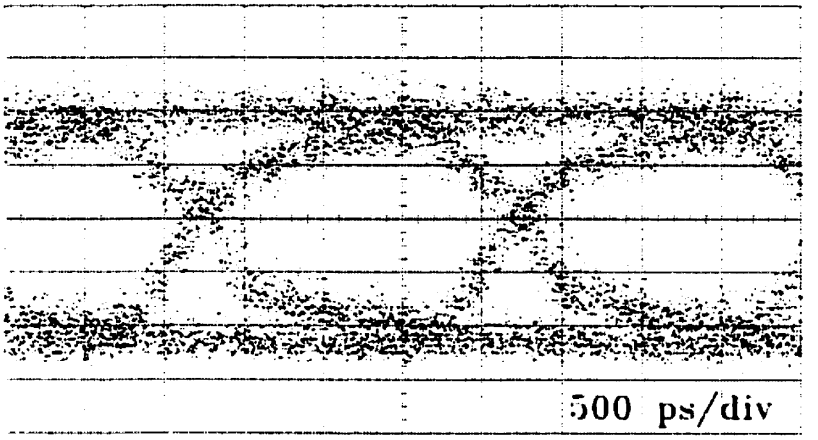

(a) 500 Mbit/s

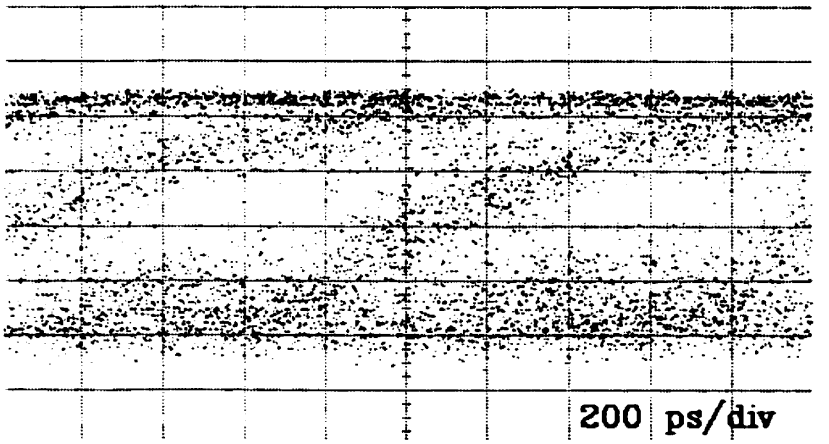

(b) 1 Gbit/s

Figure 5.3. Single channel transmission using the VCSEL array

A concern with VCSEL arrays is electrical crosstalk within the die. It can derive from thermal, electrical, or optical parasitic paths [3]. Electrical crosstalk may be capacitive (radiation) or resistive (leakage). Both tend to be aggravated by closely spaced devices or contacting electrodes [11]. In a well designed array, most lateral current confinement techniques should eliminate the resistive paths between devices.

5.3.2 *Receiver Bandwidth*

Similarly to the transmitter bandwidth measurements, single channel receiver operation has also been characterized. The test setup is essentially the same as in Figure 5.2 with the exception of the APD receiver being replaced by the 4X4 receiver array module and the 8X8 transmitter array being replaced a single laser transmitter. The main components of the single custom laser driver board [4] are a SDH/SONET 2.5 Gbit/s laser diode driver and a Honeywell VCSEL packaged in TO-46 can. Figure 5.4 shows an eye diagrams for the receiver at 500 Mbits/s and 700 Mbits/s. The average optical power at each receiver is approximately 160 μW.

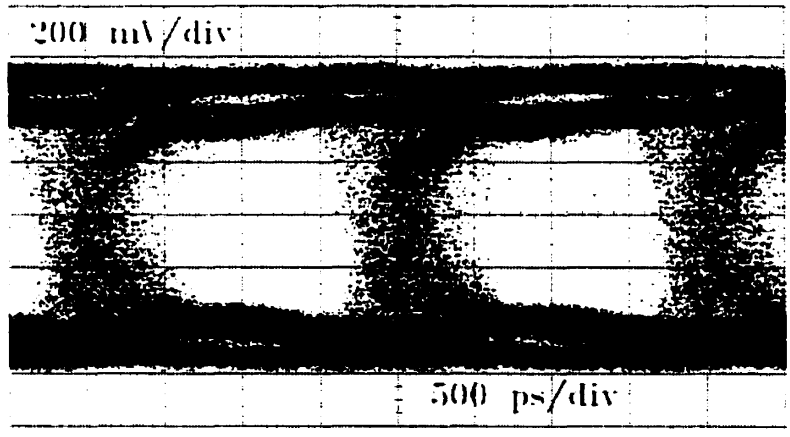

(a) 500 Mbit/s

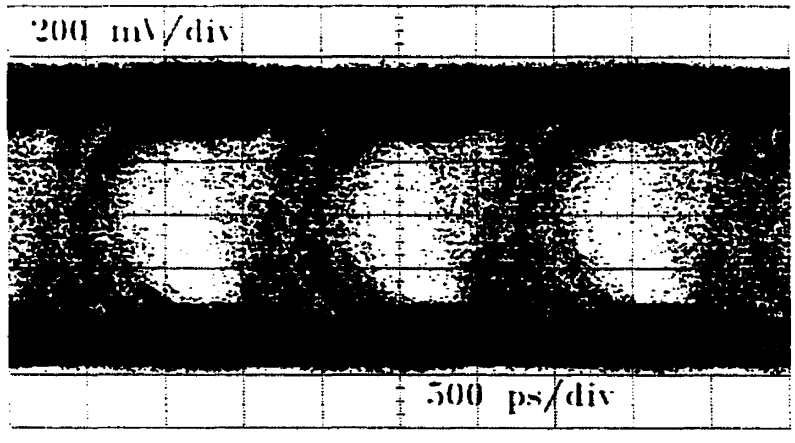

(b) 700 Mbit/s

Figure 5.4. Single-channel transmission using the receiver

As a reference, Figure 5.5 shows, under the same biasing conditions as in the setup with the 4X4 receiver, that the laser driver board is capable of producing an open eye diagram at 1 Gbit/s. From Figure 5.4 the fidelity of the receiver is seen to degrade above 500 Mbit/s. Packaging might somewhat limit the maximum bandwidth but it is likely that the receiver was mostly limited due to an excessive MSM photodetector capacitance [6]. Alteration of the detector structure may allow operation up to the designed 1 Gbit/s [6].

Figure 5.5. Eye pattern at 1Gb/s from the optical source used to test the receiver

5.3.3 Aggregate Bandwidth

Figure 5.6 shows the experimental set-up of the entire system. As in the previous section the HP data generator and the HP digitizing oscilloscope are used to generate and display the results. All ten channels were operated simultaneously with a 2^{23} - 1 PRBS. The oscilloscope enables only four simultaneous readings. Electrical signals into and out of the breakout boards are fed through high bandwidth SMA cables. Through the use of set-screws and with rotational alignment light from all 10 available VCSELs was aligned onto the detector array through the FIG. The bias for each VCSEL was adjusted to optimize the overall performance i.e. for the average power on a detector to yield the best results. On average each VCSEL was emitting somewhere between 300 and 600 μW of power and each detector was receiving approximately 160 μW. Figure 5.7, shows a typical eye diagram for 4 adjacent channels operated at 250 Mbit/s and 500 Mbits/s. A single channel with a signal clock of 1 Gbit/s was also successfully transmitted. To

minimizing thermal crosstalk, the experimental operating conditions were maintained at 25°C and a small fan favored heat dissipation at the transmitter side. The persistence time on Figure 5.7 (a) was more than a minute.

The eye diagrams in Figure 5.7 (a) are well open for an aggregate bandwidth of 2.5 Gbit/s. The fidelity of the system above 250 Mbit/s per channel was mostly limited by electrical crosstalk and noise in the transmitter electronics. All channels are triggered with the same trigger and the noticeable time delays from one channel to the other are a result of different path lengths on the PCB boards. Bending the image guide does not lead to any measurable performance reductions. However shaking the image guide adds perceptible noise to the eye diagrams. This is likely caused by power fluctuation on the detectors due to mechanical instability.

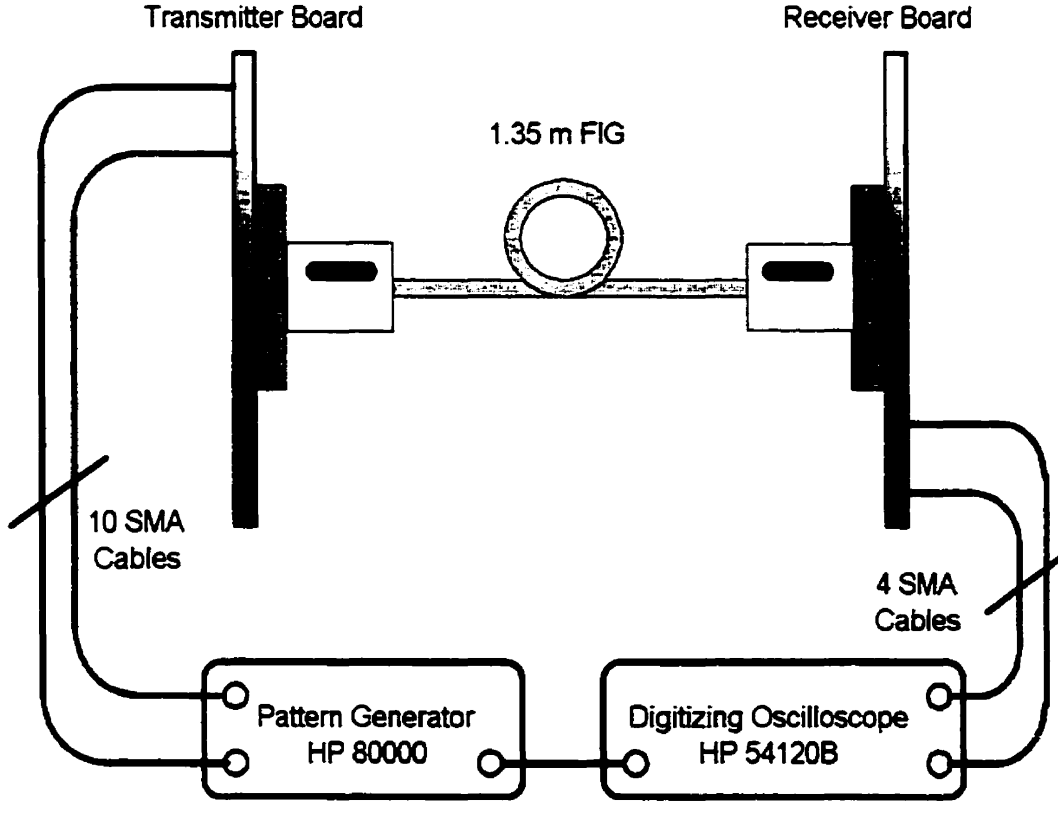

Figure 5.6. Schematic of the test set-up

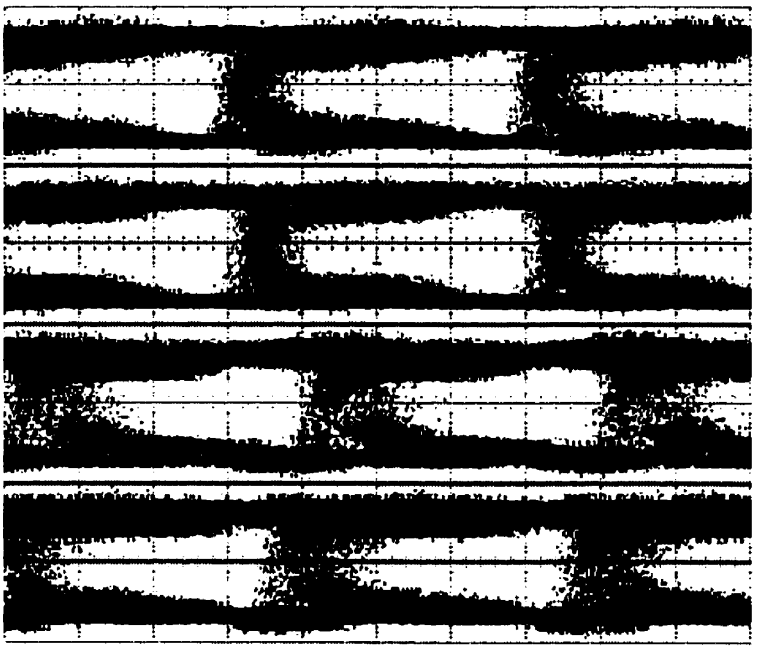

1 ns/div

(a) 250 Mbit/s

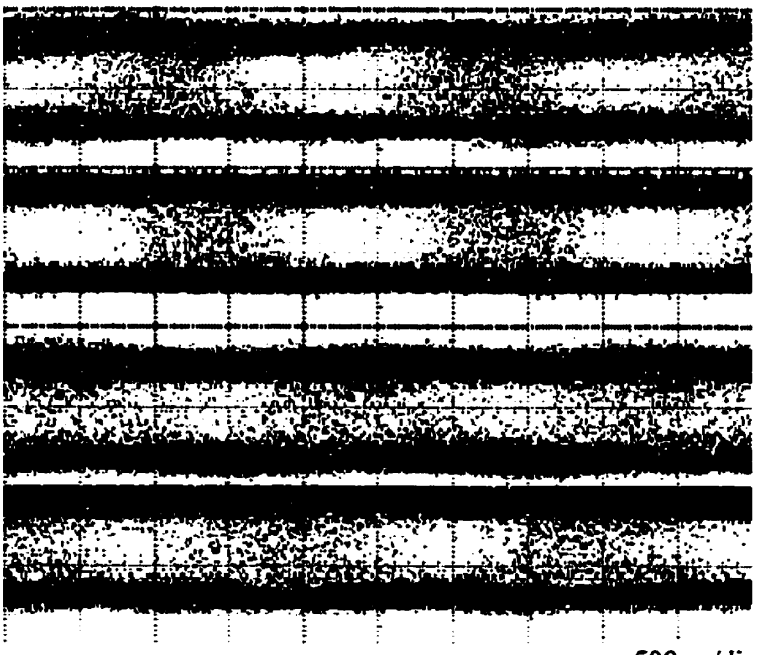

500 ps/div

(b) 500 Mbit/s

Figure 5.7. Eye diagram for 4 adjacent channels

Modal noise is a significant impairment in multi-mode fiber links and the modal noise is characterized by a speckle pattern. The speckle patterns are formed by the interference of

the modes from a coherent source [5]. In general, due to mechanical disturbances in a fiber caused by the environment or fluctuations in the lasing spectrum of the optical source, the speckle pattern varies with time, leading to signal power fluctuations and a bit error floor at the receiver. Multimode fibers in the FIG will support a number of propagating optical modes, these modes may coherently interfere at the receiver and cause its performance to degrade. The optical link, however, should be fairly immune to modal noise since the VCSEL array is a multi-transverse mode source.

Another major impairment in parallel fiber optic components is electrical crosstalk. In general, crosstalk is the result of the tight package layout of the multichannel high-speed electrical components. It is particularly severe at the receiver where the signal levels are relatively small. Significant amplification might be required and crosstalk might be a critical problem with the receivers. Another serious concern with the receiver is that the light not incident on the photodetectors illuminates the GaAs or in general silicon components and the resultant photocurrents create electrical noise and may alter device characteristics [7].

Relative intensity noise (RIN), resulting from laser spontaneous emissions, is an important quantity related to SNR. A very low value of RIN is desirable. A rate equation analysis shows that over a large operating range, the RIN of semiconductor lasers decreases with increasing laser power [8]. To decrease the RIN it would be convenient to increase the VCSEL bias, however the receiver circuit is designed with a decision threshold level less than 200 μW and provides a limited adjustment of the threshold +/- 20 μW [6]. Therefore increasing the average power leads to duty cycle distortion at the output of the system.

The imposed power constraint of the detectors also leads to biasing complications. Since an AC voltage modulation is used, the VCSEL power moves back and forth on the LI curve from a biasing point. When going down the LI curve, it potentially reaches the VCSEL threshold and creates undesirable turn-on delay. Looking closely at the eye diagram of Figure 5.7 it possible to suspect some turn-on delay. A simple solution would

be to attenuate the optical power, but due to the compactness of the optical system; space for an optical filter was not available.

For this kind of a system it is typically convenient to compare the known input with an error detector. The error detector records the number of errors and then ratios this to the number of bits transmitted. This figure of merit is called bit-error ratio, defined as:

$$BER = E(t) / N(t) \qquad \text{Equation 5.1}$$

where BER is the bit error ratio, E(t) is the number of error bits recorded over time t and N(t) is the total number of bits transmitted in time t. BER is a statistical parameter, if errors occur in bursts caused by nonrandom effects such as channel crossatlk or external interference, this simple measure might not be adequate. A bit error ratio of 10^{-9} is often considered the minimum acceptable bit error ratio for telecommunication applications. Data communications have more stringent requirements where 10^{-13} is often considered a minimum [9]. Comparing the eye diagrams of Figure 5.7 to other published eye diagrams with a corresponding BER [11], suggests BER better than 10^{-11}. A proper bit-error-ratio tester (BERT) must be used for an adequate result.

All the channels do not perform identically, the differences are not significant but they are none the less perceptible. Although each VCSEL on the array has slightly different characteristics, most of the performance discrepancies result form variations in transmitter board traceline impedance, causing signal reflection, and parasitic capacitance associated with each channel [10].

5.4 Measurements

As described in chapter 3, insertion loss into a FIG is spot size dependent. The knowledge of optical spot size is also important at the photodetector plane and therefore spot size measurement will be presented in the next section. Other system specific

properties such as power throughput and optical crosstalk will be shown in sections 5.4.2 and 5.4.3.

5.4.1 Spot Sizes

One of the design objectives was to keep spot sizes below 70 μm to accommodate the 75 μm diameter detectors. Figure 5.8 shows the spot pattern at the input of the image guide (i.e. after imaging through the transmitter optics.). Spot quality is good and there is no discernible geometric distortion. Figure 5.9 shows the output spot pattern after transmission through the image guide. As expected, each channel has been coupled into several fibers. The input pattern was also maintained during the transmission through the image guide. A calibrated and linear Hitachi model CCD camera was used to measure spot sizes. A the front face of the image guide the average measured spot diameter was found to be between 30-50 μm. The spot sizes at the detector were slightly larger and are estimated to be 40-70 μm. This remains within the constraints imposed by the 75 μm diameter detectors.

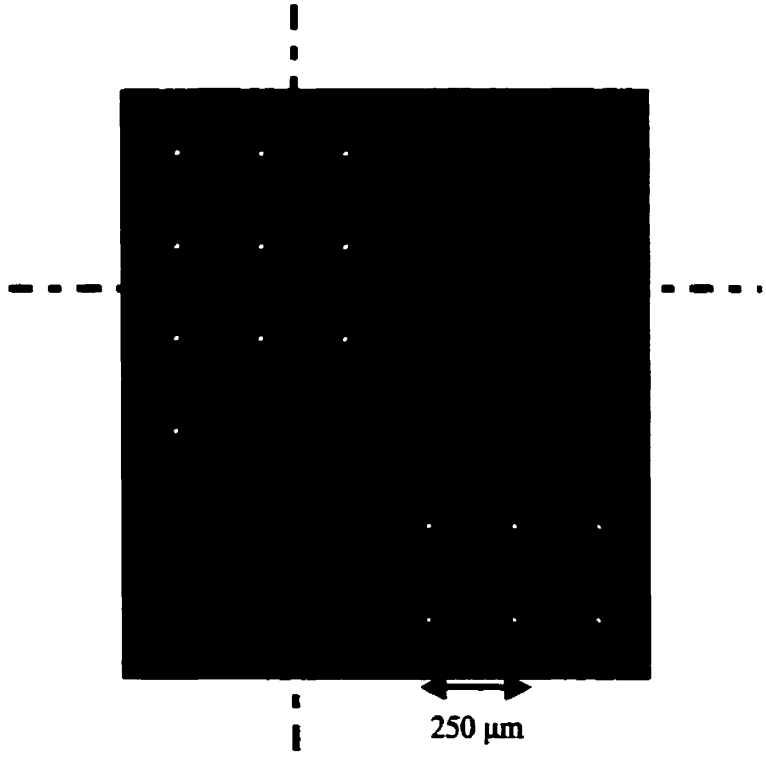

Figure 5.8. Spot pattern at image guide input face

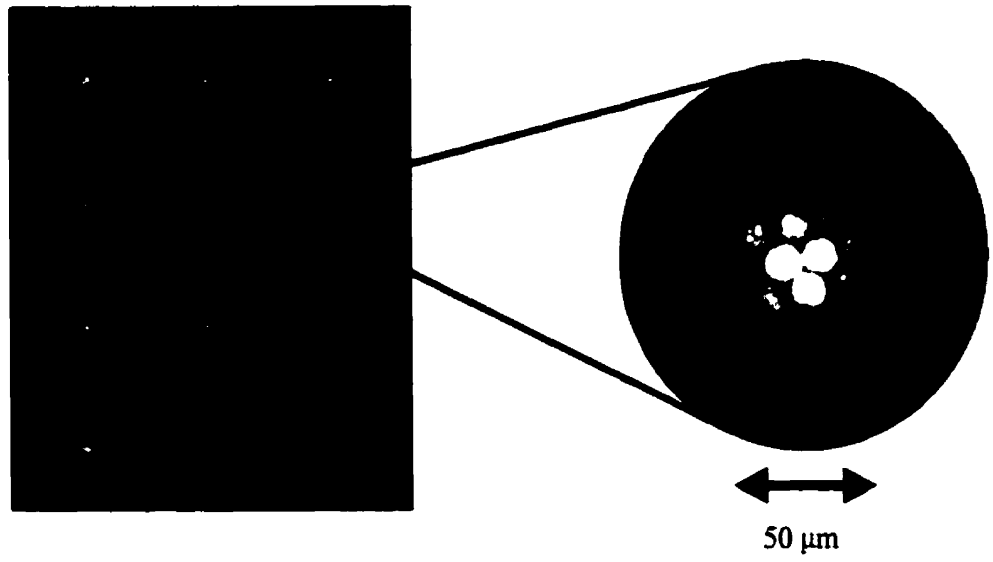

Figure 5.9. Spot pattern after transmission through image guide

The increase in spot size can be attributed to several factors. First, as discussed in chapter 3, spot spreading within the FIG can contribute to an enlargement of the spot. Secondly, the FIG contains multimode fibers which may not have identical bending and twisting. Thus, such a FIG may contain non-uniform mode coupling, thereby generating a somewhat bigger illumination than at the input i.e. the divergence angle of the VCSEL. In general for long length propagation the light will exit with an angle corresponding to the numerical aperture of the FIG i.e. 0.55. The coupling optics are fast enough to collect the light but aberration further contributed to the increase of the spot at the detectors.

5.4.2 Power Throughput

A typical loss-distribution analysis is shown in Figure 5.10. A Newport 1835-C power meter was inserted between the different optical elements and recorded power levels. The two plots represent the best and worst case scenarios as determined with repeatability tests compiled through several channels. The dominant source of loss was in the coupling

to the image guide. The lenses are coated with a single layer MgF_2 and at 830 nm are specified to contribute at normal incidence a maximum reflectance of 2 %, which is consistent with the measured results. Overall, the total power loss varies depending on the channel and the position of the spot with respect to the FIG. The total loss was measured to be between 3 and 5 dB. This loss includes approximately a 2 dB/m attenuation within the FIG as shown in chapter 3. Most of the coupling loss can be attributed to the fill-ratio of the image guide, which is approximately 55 %. Other experiments have reported similar power efficiencies i.e. a 5.7-dB loss in transmitting optical signals from a VCSEL through a glass FIG [12]. That result contained tapering loss, bending loss, interpixel interference loss and loss caused by the fill ratio of the FIG.

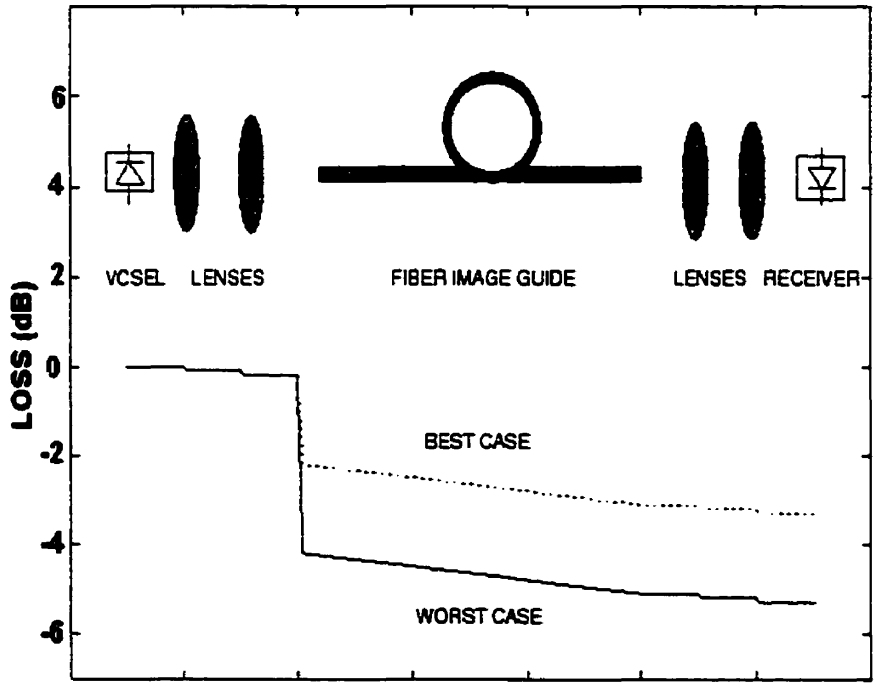

Figure 5.10. Insertion loss distribution

5.4.3 Optical Crosstalk

Optical crosstalk may be the most difficult problem to solve, especially in free-space interconnected arrays or in cases where the optical coupling loss to the desired medium (e.g., fiber) is large. In both cases stray light tends to be generated, and unless care is

exercised, this may find its way to adjacent receiver elements. It is generally desirable to avoid significant scattering from optical elements or the generation of high-order lateral modes. Non-ideal coupling optics can also create problems.

In order to characterise the optical crosstalk incurred in the system, we define crosstalk as the DC signal level captured on a detector from an adjacent channel with respect to the signal level. This approach prevents measuring other forms of crosstalk such as inductive and capacitative crosstalk between channels and leakage between VCSELs due to a finite resistance between them. The response was measured by simulating the 75 μm detectors with a somewhat larger 100 μm diameter pin-hole resulting in a conservative measurement.

Figure 5.11 illustrates the experimental set-up to measure optical crosstalk. A single channel was biased and the pin-hole was translated across the image plane. To simulate the photodetectors, the pin-hole was carefully aligned to coincide with the plane of the detectors. A Newport 1835-C optical power meter was used to measure optical power transmitted through the pin-hole and Figure 5.12 presents the distribution with respect to position in one axis. The other axis was adjusted so that as to ensure the spot passes through the center of the pin-hole. Temperature on the VCSEL die was fixed to 24°C for the duration of the measurement. Optical crosstalk from the closest neighboring channel i.e. the channel 250 μm away from the maximum optical power position can be estimated at less than –33dB. The total contribution from the four neighboring channels can be estimated at less than –27 dB. Similarly it is possible to conclude that this optical system would equally support VCSELs with a 125 μm pitch suggesting a single channel crosstalk of less than -26 dB. This result compares adequately with other reported result were with a 125 μm VCSEL pitch, less than -30-dB crosstalk was obtained with a glass FIG [13].

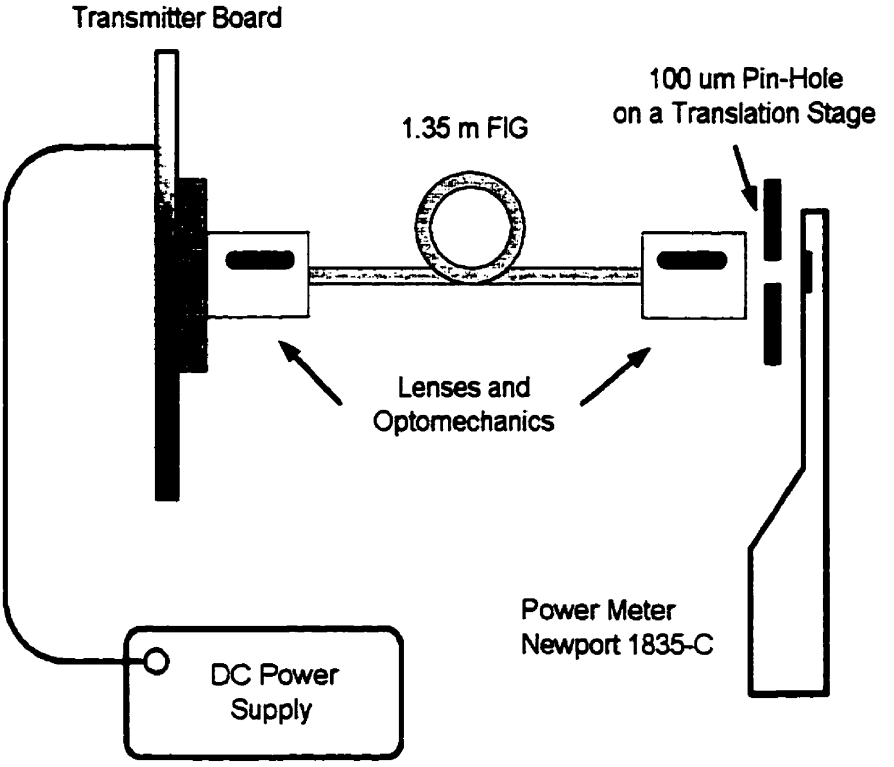

Figure 5.11. Schematic of the crosstalk test set-up

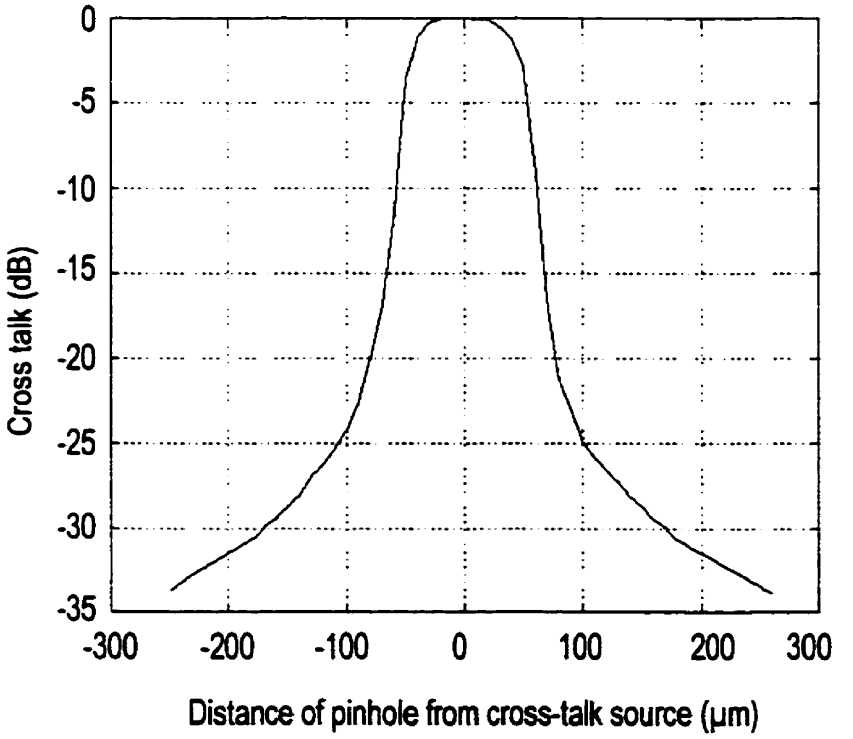

Figure 5.12. Crosstalk into a 100 μm diameter aperture as a function of distance from crosstalk source

5.5 References

1. W. Hsiao, "Integration and Characterization of an MSM array for Free-Space Optical Backplanes", Master Thesis, 1996.

2. C.T. Tsai, "Package Inducatance Characterization at High Frequencies", *IEEE Trans. Comp. Pack. and Manufact. Tech.*, vol. 17, no 2, pp.175-181, May 1994.

3. L.A. Coldren and B. J. Thibeault, Optical Fiber Telecommunications Volume IIIB, edited by P. Kaminow, T. L. Koch, Academic Press, San Diego, chapter 6, 1997.

4. M. Ayliffe, Laser Driver Board Operating Instructions, Internal Documentation, March 1999.

5. J.M. Senior, Optical Fiber Communications: Principles and Practice, Prentice-Hall International, Inc., London, (1985).

6. J.F. Ahadian, "A Monolithic Very Large Scale Optoelectronic Integrated Circuit Technology" Massachusetts Institute of Technology, Ph.D. Thesis, 1999.

7. F.B. McCormick, in Photonics in Switching, Volume II, edited by J.E. Midwinter, Academic Press, Inc., Boston, pp. 169-250, 1993.

8. G.P. Agrawal and N. K. Dutta, Semiconductor Lasers, Thomson publishing, Inc., New York, Chapter 6, 1993.

9. D. Derickson, Fiber Optic Test and Measurment, Prentice-Hall, Inc. New Jersey, 1998.

10. N.H. Kim, "2D free-Space Optical Backplane Using Vertical-Cavity Surface-Emitting Laser", McGill University, Master Thesis, 1996.

11. R. Nagarajan, W. Sha, B. Li, and R. Craig, "Gigabyte/s Parallel Fiber-Optic Links Based on Edge Emitting Laser Diode Arrays", *J. of Lightwave Tech.*, vol. 16, no. 5, pp. 778-787, May 1998.

12. Y. Li, T. Wang, and S. Kawai, "Distributed crossbar interconnects with vertical-cavity surface-emitting laser-angle multiplexing and fiber image guides", Appl. Opt. 37, pp. 254-263, 1998.

13. H. Kasada, M. Kajita, Y. Li and Y. Sugimoto, "A two-dimensional optical parallel transmission using a vertical-cavity surface-emitting laser array module and an image fiber." IEEE Photon. Tech. Lett. 9, pp. 253-255, 1997.

Chapter 6

Conclusion and Future Directions

6.1 Review

This thesis has presented the motivation for high-density 2D parallel optical interconnects. Most current high-speed parallel optical data links have been demonstrated with 1D fiber ribbons and fiber image guide based technology was proposed to replace current coaxial-cable bundles or to become an alternative to fiber arrays. In chapter 2, active optoelectronics devices required for the realization of such optical links were proposed. General properties and structures of semiconductor lasers and photodetectors were described along with high-speed modulation requirements. Specific characteristics of an 8X8 VCSEL array and monolithic receiver were presented as well as beam propagation fundamentals required for a proper design of the optical system. VCSEL multi transverse mode beam characteristics were observed and the divergence angle was found to vary from 18 to 24 degrees as the injected current is increased. Single transverse mode VCSELs are necessary in order to facilitate the design and to increase the efficiency of optical systems. MSM photodetectors with their planar structures offered several fabrication advantages but their low responsivity and excessive capacitance limited high-speed operation.

In chapter 3, fiber image guides were examined with respect to their transmission characteristics. Input spot size was found to affect the power uniformity and coupling efficiency into the fiber image guide. A spot size of 50 μm was found to give a 10% power uniformity. Since uniform and repeatable coupling efficiency is highly desirable, it was determined that fiber cores should be as small as possible to enable each channel to travel on several cores. A higher fill ratio is also necessary and it can be achieved by decreasing the fiber pitch i.e. the spacing between the fiber cores. A typical attenuation

for an image guide was measured at less than 2.5 dB/m and spot spreading was found to be limited to one adjacent fiber. For VCSEL based applications the NA of the FIG should be reduced to match the divergence of the VCSELs. A NA of 0.2 to 0.25 would be adequate, and it would prevent to have a high divergence angle at the output of the FIG. Overall properties of fiber image guides such as bending loss, dispersion and back reflections were also examined and the results are very encouraging. Since a channel travels over several cores, the desired density of dark/grey fibers must not exceed one fiber per channel and the current failure density easily exceeds this specification. Although fiber image guides can be manufactured in different sizes and lengths while maintaining good flexibility they are most likely limited to point-to-point applications or short-distance large-array bandwidth optical communications.

In chapter 4 and 5, the design, construction and performance of the bit-parallel demonstrator was presented. It was determined that spot size should be selected to accommodate the detector area. To achieve spot sizes smaller than 75 μm at the plane of the 75 μm photodetectors, a spot size restriction of 50 μm was imposed at the input of the FIG. With spot sizes smaller than 50 μm, transmitted power variations required to individually adjust the bias on each VCSEL. For this reason, it was concluded that the size of the individual image guide cores should be decreased as well as the pitch between them. Active alignment of the FIG was necessary to interconnect the transmitter and receiver optoelectronics. To summarise the results, light from a two-dimensional VCSEL array was transmitted through a 1.35 m fiber image guide and onto a detector array. Up to ten channels were transmitted simultaneously at 250 Mbit/s with less than -32 dB of optical crosstalk per adjacent channel. A total optical throughput of -3 to -5 dB was measured. Dispersion and skew were not observed over the relatively short length of fiber image guide used in the system. These obtained results indicate that FIG based optical data links may be achieved in the near future.

6.2 Ongoing and Future Work

High bandwidth parallel optical systems require substantial further developments and enhancements. The results and discussion presented in this thesis have helped to identify specific needs and limitations that must be addressed in order to benefit the development of practical system implementations. The following sections outline some areas of future study.

6.2.1 Optoelectronic Technology

For transmitters and receivers, integrated two-dimensional optoelectronic VLSI (OE-VLSI) devices should significantly lower costs while improving device reliability. This can be achieved with monolithic integration of semiconductor optical devices with semiconductor electronics [1] or it can also be achieved by hybridization of optical devices with silicon electronics requiring minimal changes to standard CMOS VLSI processing techniques [2]. Although these technologies are currently being demonstrated they still require a few years of development and refinement.

6.2.2 Future FIG Based Interconnects

The coupling optics in the FIG based interconnect consisted of commercially available objective lenses. The main challenge in the optical design was the need for low-aberration, wide-field, high-resolution lenses that are compact and inexpensive. To achieve diffraction-limited performance over wide fields at low f-numbers generally requires multi-element lenses and precise element mounting. Further for image guide coupling it is also desirable to have predictable circular spot. For these reasons an alternative method of coupling must be investigated.

The most foreseeable alternatives are to use micro-optics or face-plates (butt-coupling through a slab of image guide). For practical systems the fiber image guides should be interconnected with push-pull type connectors. To accommodate such connectors passive

alignment techniques such as ball guide die-bonding [3] must be addressed or precise connectors must be manufactured. The fabrication of precise connectors requires the accurate control of the exact location of the fiber bundle within the rigid outer jacket. Anti-reflection coatings on the optical components should be considered as well as the use of index matching fluids between the VCSELs and face-plates for example. For bi-directional systems, in which transmitting and receiving channels are interleaved [2], careful alignment techniques which account for the tilt of the FIG or dedicated connectors will be required to alleviate the need for positioning optomechanics. These requirements might lead to a higher level of packaging complexity.

6.2.3 Scalability and Additional FIG Related Issues

To transmit data from all 64 VCSELs an ASIC capable of driving the entire array needs to be developed as well as a better packaging method. As for the receiver, the primary limitation lies in the cost of scaling the 4X4 array due the escalation of the die area to roughly 40 mm^2 [4]. This scaling is necessary to support the many bondpads consumed by the ECL outputs and the accompanying power and ground connections [4]. The scalability of the FIG transmission area is not an obstacle since 1 cm^2 image guides are currently available with good flexibility.

With a continued increase in demand for a higher number of channels, larger arrays of VCSELs and detectors may be required in the future. To accommodate this higher number of channels the I/O density will likely increase faster than the chip size and a 62.5 μm pitch is quite foreseeable. Such a pitch will impose design constraints on the transmitter and receiver optoelectronics. For such a channel density, spot sizes will have to decrease and FIGs will have to be manufactured with smaller cores and pitches to maintain good transmission characteristics. Also, smaller cores, near single mode sizes will enable longer transmission lengths and/or higher data rates.

To conclude, this work has demonstrated proof of concept of integrating fiber image guides in parallel optical data links. Fiber image guides have been demonstrated to be

excellent optical component for board level to LAN level optical interconnections that use infrared array devices. Embedding fiber image guides yields a well packaged optical interconnect solution. If the simplicity in the connectorization methods is achieved we might assist in their insertion into practical applications.

6.3 References

1. K.L. Lear, "Technologies for Highly Parallel Optoelectronic Integrated Circuits", *IEEE GaAs IC Symposium. 16th Annual. (Technical Digest 1994)*, New York, NY, pp. 201-206. 1994.

2. D.V. Plant, J.A. Trezza, M. Venditti, E. Laprise, J. Faucher, K. Razavi, M. Chauteauneuf, T. Maj, A. Ghanem, F. Thomas-Dupuis, P. Sehgal, A.G. Kirk, and W. Lao, "A 256 Channel Bi-Directional Optical Interconnect Using VCSELs and Photodiodes on CMOS", *Submitted conference paper for OC 2000*, Quebec, Quebec, Canada, 2000.

3. H. Kosaka, "Smart Integration and Packaging of 2-D VCSEL's for High-Speed parallel Links", *IEEE J. of Selected Topics in Quant. Elect.*, vol. 5, no. 2, pp.184-192, 1999.

4. J.F. Ahadian, "A Monolithic Very Large Scale Optoelectronic Integrated Circuit Technology" Massachusetts Institute of Technology, Ph.D. Thesis, 1999.